

Ancient TL

A periodical devoted to Luminescence and ESR dating

Institute of Geography and Earth Sciences, Aberystwyth University,
Ceredigion SY23 3DB, United Kingdom

Volume 30 No.2

December 2012

Dose response curve of the ESR signal of the Aluminum center in quartz grains extracted from sediment

M. Duval _____ 41

Assessing the influence of the cavity temperature on the ESR signal of the Aluminum center in quartz grains extracted from sediment

M. Duval and V. Guilarte Moreno _____ 51

A novel beta source design for uniform irradiation in dosimetric applications

D.Richter, R. Pintaske, K. Dornich and M. Krbetscheck _____ 57

Thesis abstracts

X. J. Liu _____ 65

D. Moreno _____ 65

R. Lyons _____ 66

R. Sohbati _____ 67

C.M. Neudorf _____ 67

D. Popov _____ 68

Bibliography _____ 71

Obituary

M.R. Krbetschek _____ 83

Announcements

UK Luminescence and ESR Meeting 2013, St. Andrews _____ 85

Book of abstracts for UK Luminescence meeting 2012 _____ 86

ISSN 0735-1348

Ancient TL

Started by the late David Zimmerman in 1977

EDITOR

G.A.T. Duller, Institute of Geography and Earth Sciences, Aberystwyth University, Ceredigion SY23 3DB, United Kingdom (ggd@aber.ac.uk)

EDITORIAL BOARD

I.K. Bailiff, Luminescence Dosimetry Laboratory, Dawson Building, University of Durham, South Road, Durham DH1 3LE, United Kingdom (ian.bailiff@durham.ac.uk)

R.DeWitt, Department of Physics, East Carolina University, Howell Science Complex, 1000 E. 5th Street Greenville, NC 27858, USA (dewittr@ecu.edu)

S.H. Li, Department of Earth Sciences, The University of Hong Kong, Hong Kong, China (shli@hku.hk)

R.G. Roberts, School of Geosciences, University of Wollongong, Wollongong, NSW 2522, Australia (rgrob@uow.edu.au)

REVIEWERS PANEL

R.M. Bailey, Oxford University Centre for the Environment, Dyson Perrins Building, South Parks Road, Oxford OX1 3QY, United Kingdom (richard.bailey@ouce.ox.ac.uk)

J. Faïn, Laboratoire de Physique Corpusculaire, 63177 Aubièrre Cedex, France (jean.fain@wanadoo.fr)

R. Grün, Research School of Earth Sciences, Australian National University, Canberra ACT 0200, Australia (rainer.grun@anu.edu.au)

T. Hashimoto, Department of Chemistry, Faculty of Sciences, Niigata University, Niigata 950-21, Japan (thashi@curie.sc.niigata-u.ac.jp)

D.J. Huntley, Department of Physics, Simon Fraser University, Burnaby B.C. V5A1S6, Canada (huntley@sfu.ca)

M. Lamothe, Dépt. Sci. de la Terre, Université du Québec à Montréal, CP 8888, H3C 3P8, Montréal, Québec, Canada (lamothe.michel@uqam.ca)

N. Mercier, Lab. Sci. du Climat et de l'Environ, CNRS-CEA, Av. de la Terrasse, 91198, Gif sur Yvette Cedex, France (norbert.mercier@lscce.cnrs-gif.fr)

D. Miallier, Laboratoire de Physique Corpusculaire, 63177 Aubièrre Cedex, France (miallier@clermont.in2p3.fr)

S.W.S. McKeever, Department of Physics, Oklahoma State University, Stillwater Oklahoma 74078, U.S.A. (stephen.mckeever@okstate.edu)

A.S. Murray, Nordic Laboratory for Luminescence Dating, Risø National Laboratory, Roskilde, DK-4000, Denmark (andrew.murray@risoe.dk)

N. Porat, Geological Survey of Israel, 30 Malkhe Israel St., Jerusalem 95501, Israel (naomi.porat@gsi.gov.il)

D. Richter, Lehrstuhl Geomorphologie, University of Bayreuth, 95440 Bayreuth, Germany (daniel.richter@uni-bayreuth.de)

D.C.W. Sanderson, Scottish Universities Environmental Research Centre, Scottish Enterprise Technology Park, East Kilbride G75 0QF, UK (David.Sanderson@glasgow.ac.uk)

A.K. Singhvi, Rm 203, Physical Research Laboratory, Navrangpura, Ahmedabad 380009, India (singhvi@prl.res.in)

K.J. Thomsen, Radiation Research Division, Risø National Laboratory for Sustainable Energy, Technical University of Denmark, DK-4000, Roskilde, Denmark (krth@risoe.dtu.dk)

Ancient TL

A periodical devoted to Luminescence and ESR dating

Web site: <http://www.aber.ac.uk/ancient-tl>

Institute of Geography and Earth Sciences
Aberystwyth University SY23 3DB
United Kingdom

Tel: (44) 1970 622606

Fax: (44) 1970 622659

E-mail: ggd@aber.ac.uk

Dose response curve of the ESR signal of the Aluminum center in quartz grains extracted from sediment

M. Duval

Centro nacional de investigación sobre la evolución humana (CENIEH), Paseo de Atapuerca s/n, 09002-Burgos, Spain (e-mail: mathieu.duval@cenieh.es)

(Received 11 May 2012; in final form 31 October 2012)

Abstract

A single saturating exponential (SSE) function is classically used in ESR dating to fit the experimental ESR data points derived from the aluminum (Al) center in quartz. However, this function has some obvious limits as it does not accurately fit the data points of the dose response curve. This results in unreliable equivalent dose (D_E) values which are highly dependent on the maximum irradiation dose.

Dose response curves of Al center in quartz show that the dose response data contain at least two components: a first one dominating at low dose (usually < 5 kGy) and saturating quite quickly and a second one dominating at higher doses with an almost linear behavior. These data are more appropriately fitted with a function combining an exponential with a linear term (EXP+LIN). Two variations of the EXP+LIN function were studied, each one corresponding to distinct physical assumptions. Since it is still unclear which one should be preferred, the mean D_E value extracted from the fitting of the two equations may be reasonably considered as the most reliable estimate of the true D_E value. In addition, to ensure accurate fitting of the linear part, it is important to have at least three data points at high doses (>10 kGy). It is also suggested to pool all the ESR intensities derived from repeated ESR measurements of each aliquot in the fitting process, in order to reduce the error in the D_E value.

Introduction

In ESR as well as in luminescence dating, the selection of the mathematical function to fit the experimental data point has a direct impact on the calculated equivalent dose (D_E) value. This is even more crucial when working with the additive dose method, which requires back extrapolation of the data to the X-axis. In the field of ESR dating, this topic has been widely discussed for carbonates (e.g. Grün et al., 1990; Barabas et al., 1992; Walther et al., 1992; Hoffmann et al., 2003) and fossil tooth enamel (Lee et al., 1997; Rink and Schwarcz, 1994; Duval et al., 2009). In contrast, there is little information available about the mathematical description of the

dose response curves of the aluminum (Al) center in sedimentary quartz.

Since the first applications of ESR to date optically bleached quartz grains extracted from sediment (e.g. Yokoyama et al., 1985), a single saturating exponential (SSE) function has been systematically used to fit the experimental Al-ESR dose response data (e.g. Rink et al., 2007; Liu et al., 2010; Voinchet et al., 2010). However, this function does not accurately describe the behavior of the Al-ESR signal with the absorbed dose, since it shows systematic deviations from experimental data sets. In addition, studies on the optical bleaching kinetics of the Al signal show that at least two components are involved in the process (Voinchet et al., 2003). It is therefore reasonable to explore the potential of a similar approach including more than one component to describe the creation of Al centers with absorbed dose. In this paper, the limits of the SSE function are discussed and the appropriateness of an alternative fitting approach combining the SSE function with a linear term (EXP+LIN) is assessed.

Material and method

The dose response curves (DRCs) of the Al center from 15 quartz samples were selected. The sediment samples were collected in diverse Plio-Pleistocene geological contexts from various areas of the Iberian Peninsula. Quartz grains were extracted according to a protocol similar to that described in Voinchet et al. (2007). Depending on the sample, irradiation involved 11 to 14 dose steps with maximum irradiation doses (D_{max}) between 23,100 and 40,000 Gy (Table 1). The residual ESR intensity of the artificially bleached component was first subtracted from the DRC values and then each DRC was normalized to the ESR intensity of the corresponding natural aliquot, to obtain comparable data. All ESR data are available in supplementary information. Two fitting functions were tested:

Single saturating exponential (SSE) function

The SSE function was first proposed by Apers et al. (1981), to account for saturation effects of the ESR

| Sample | Site/Outcrop, Location | Number of dose steps | D_{\max} (Gy) |
|--------|---|----------------------|-----------------|
| 1 | Huescár-1, Guadix-Baza basin (Southern Spain) | 14 | 40000 |
| 2 | Huescár-1, Guadix-Baza basin (Southern Spain) | 13 | 40000 |
| 3 | Fuente Nueva-3, Guadix-Baza basin (Southern Spain) | 11 | 25000 |
| 4 | Vallparadís, Terrassa (Eastern Spain) | 11 | 25000 |
| 5 | Vallparadís, Terrassa (Eastern Spain) | 11 | 25000 |
| 6 | Villarroya, Ebro basin (Northern Spain) | 12 | 25000 |
| 7 | Villarroya, Ebro basin (Northern Spain) | 12 | 25000 |
| 8 | Tejares, Duero basin (Northern Spain) | 12 | 25000 |
| 9 | Tejares, Duero basin (Northern Spain) | 12 | 25000 |
| 10 | Barranco León, Guadix-Baza basin (Southern Spain) | 11 | 24000 |
| 11 | Atapuerca Sima del Elefante, Duero basin (Northern Spain) | 11 | 23300 |
| 12 | Atapuerca Sima del Elefante, Duero basin (Northern Spain) | 11 | 22100 |
| 13 | Maresa, Tajo basin (Central Spain) | 11 | 22900 |
| 14 | Valdocarros, Tajo basin (Central Spain) | 11 | 22700 |
| 15 | Cúllar de Baza, Guadix-Baza basin (Southern Spain) | 11 | 23100 |

Table 1: Details of the fifteen ESR samples.

signal at high irradiation dose. By using this function, it is usually assumed that the ESR signal is dominated by a single paramagnetic center. The SSE function may be written as follows:

$$I(D) = I_{sat} \left[1 - \exp\left(-\frac{D+D_E}{D_0}\right) \right] \quad (1)$$

where D is the absorbed dose (Gy), I is the ESR intensity (in a.u.). Three parameters are fitted: the equivalent dose (D_E), the saturation ESR intensity (I_{sat}) and the characteristic saturation dose (D_0). Sometimes $1/D_0$ is used to express the radiation sensitivity of the sample.

Exponential+linear (EXP+LIN) function

This function is made by the sum of a SSE function and a linear term. This function was first introduced by Goldberg et al. (1973) and then taken up by Levy (1985) in order to describe the formation of radiation induced species for a system where several components are involved. This function was previously used in luminescence dating (Berger, 1990; Fattahi et al., 2004), in ESR studies of corals

(Grün, 1990; Walther et al., 1992) and enamel (Duval et al., 2009), but not for quartz, until the work by Duval et al (2011). Basically, the use of this kind of function suggests that the ESR signal is the result of two main components, one dominating at low irradiation doses and saturating at relatively low doses while the other is dominating at high doses. The EXP+LIN is usually considered appropriate for systems where traps are generated during irradiation (Levy, 1985). However, it can be also interpreted as a sum of two different saturation functions, including one with such a high saturation level that it may be approximated by a straight line (Walter et al., 1992). Following the second hypothesis, the equation may be written as follows:

$$I(D) = I_{sat} \left[1 - \exp\left(-\frac{D+D_E}{D_0}\right) \right] + m(D+D_E) \quad (2)$$

There are four fitted parameters with this function: D_E , I_{sat} , D_0 and m . The latter may be considered as an estimation of the radiation sensitivity of the second component.

The fitting procedures were carried out with the Microcal OriginPro 8.5 software using a Levenberg-Marquardt algorithm by chi-square minimization. Further details can be found in the Origin 8 User Guide (2007). The data points were weighted by the inverse of the squared ESR intensity ($1/I^2$). For a discussion of the weighting of luminescence and ESR data points, see Grün and Brumby (1994) and references therein. The goodness of fit is assessed through the adjusted r-square (r^2) value, which accounts for the degrees of freedom of the system, contrary to the classical coefficient of determination r^2 (for further details see the Origin 8 User Guide).

Apparent limitations of the SSE function

Fig. 1 shows a couple of examples of DRCs (samples #1 and #6). It is already visually obvious that the SSE function does not correctly fit the ESR data points. For sample #1, the SSE function is not only inappropriate in the high dose region ($D > 25$ kGy), with modelled ESR intensities significantly lower than the experimental ones, but also in the intermediate dose region (~ 6 kGy $< D < \sim 25$ kGy), in the maximum curvature area of the SSE where experimental data are not fitted at all. Lastly, in the low dose region ($D < \sim 6$ kGy), the curve goes through almost none of the points, and the SSE passes above the natural point. A similar trend is observed for sample #6. Other examples may also be found in Duval et al. (2011).

Sometimes, the SSE function resulted in a good fit (adjusted $r^2 > 0.99$) of the experimental data, but this applied only to two samples of the present data set: samples #3 and #9 (Table 2). The corresponding

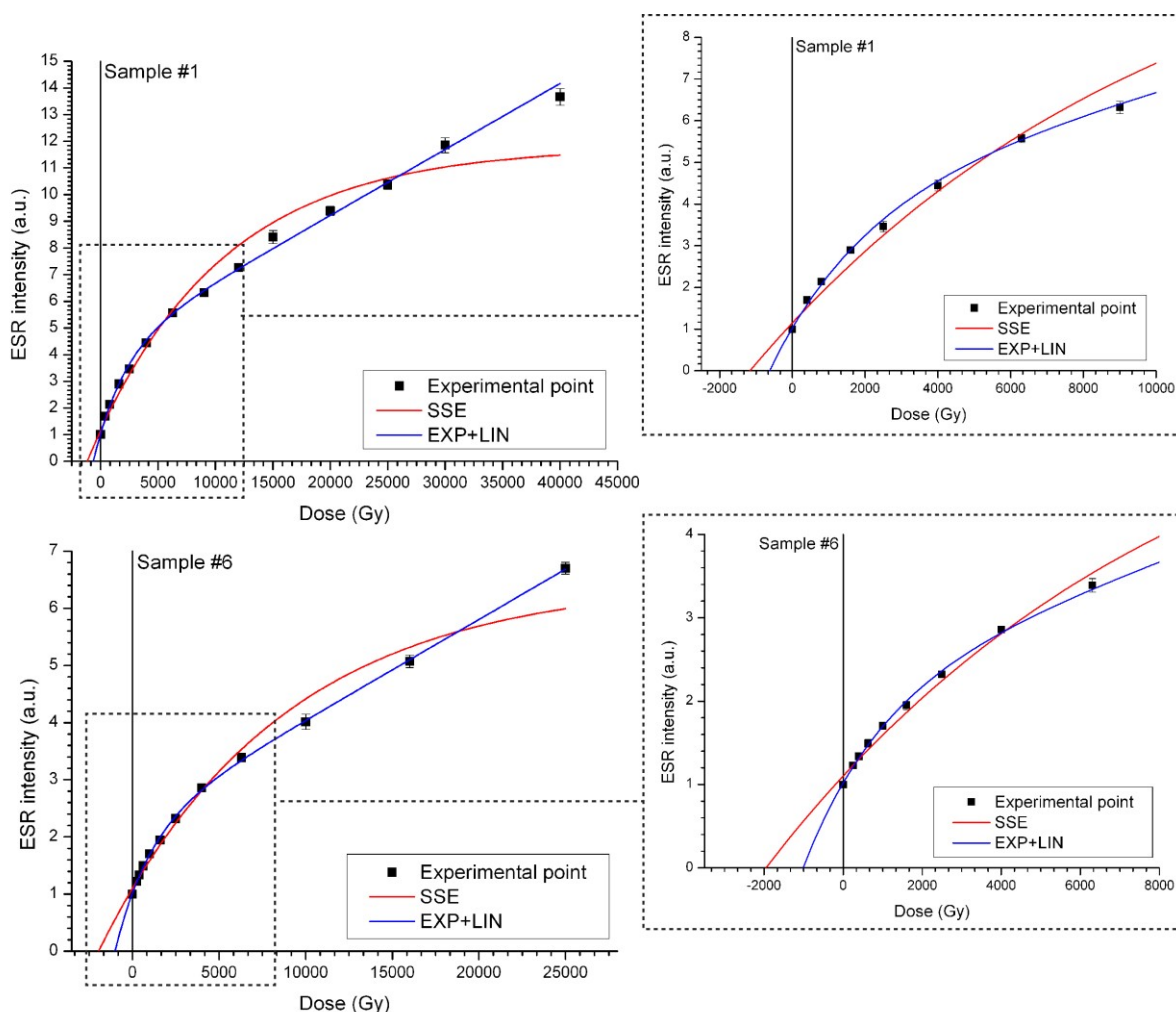


Figure 1: Examples of dose response curves (Samples #1 and #6). Mean ESR intensities were calculated from repeated ESR measurements of each sample. Errors on the ESR intensities correspond to 1 standard deviation.

| Sample number | SSE - Equation (1) | | | | EXP+LIN - Equation (2) | | | | | | | (EXP+LIN)/(SSE) | |
|---------------|--------------------|-------|-------|----------------|------------------------|-------|-------|-----------|-------|----------|----------------|-----------------|----------------|
| | D_E | \pm | % | Adjusted r^2 | D_E | \pm | % | I_{sat} | D_0 | m | Adjusted r^2 | D_E | Adjusted r^2 |
| 1 | 1166 | 180 | 15.4 | 0.97544 | 631 | 56 | 8.9 | 4.12 | 2639 | 0.000247 | 0.99708 | 0.54 | 1.022 |
| 2 | 742 | 131 | 17.7 | 0.97059 | 458 | 70 | 15.3 | 5.58 | 2707 | 0.000405 | 0.99060 | 0.62 | 1.021 |
| 3 | 1975 | 140 | 7.1 | 0.99446 | 1665 | 143 | 8.6 | 2.96 | 4541 | 0.000051 | 0.99773 | 0.84 | 1.003 |
| 4 | 2696 | 319 | 11.8 | 0.98489 | 1699 | 172 | 10.1 | 1.98 | 2982 | 0.000078 | 0.99781 | 0.63 | 1.013 |
| 5 | 4694 | 748 | 15.9 | 0.97292 | 1703 | 339 | 19.9 | 1.43 | 1862 | 0.000052 | 0.99137 | 0.36 | 1.019 |
| 6 | 1951 | 261 | 13.4 | 0.97736 | 1012 | 70 | 6.9 | 2.10 | 1986 | 0.000176 | 0.99903 | 0.52 | 1.022 |
| 7 | 1990 | 190 | 9.5 | 0.98841 | 1340 | 121 | 9.0 | 2.42 | 3114 | 0.000116 | 0.99783 | 0.67 | 1.010 |
| 8 | 3155 | 322 | 10.2 | 0.98691 | 1841 | 195 | 10.6 | 1.77 | 2820 | 0.000098 | 0.99792 | 0.58 | 1.011 |
| 9 | 2157 | 173 | 8.0 | 0.99172 | 1506 | 91 | 6.0 | 2.31 | 3492 | 0.000137 | 0.99915 | 0.70 | 1.007 |
| 10 | 1879 | 191 | 10.2 | 0.98874 | 1526 | 205 | 13.4 | 2.76 | 3719 | 0.000051 | 0.99432 | 0.81 | 1.006 |
| 11 | 1611 | 166 | 10.3 | 0.98918 | 1474 | 236 | 16.0 | 3.99 | 6093 | 0.000064 | 0.98876 | 0.91 | 1.000 |
| 12 | 2385 | 248 | 10.4 | 0.98783 | 2193 | 411 | 18.7 | 3.24 | 6463 | 0.000045 | 0.98674 | 0.92 | 0.999 |
| 13 | 2587 | 298 | 11.5 | 0.98502 | 1659 | 213 | 12.8 | 1.99 | 2745 | 0.000073 | 0.99637 | 0.64 | 1.012 |
| 14 | 1488 | 199 | 13.4 | 0.98083 | 933 | 70 | 7.5 | 2.61 | 2200 | 0.000129 | 0.99846 | 0.63 | 1.018 |
| 15 | 3228 | 364 | 11.3 | 0.98581 | 1937 | 141 | 7.3 | 1.73 | 2625 | 0.000056 | 0.99891 | 0.60 | 1.013 |
| Mean | 2247 | | 11.7 | 0.98401 | 1438 | | 11.4 | 2.73 | 3333 | 0.000118 | 0.99547 | 0.67 | 1.012 |
| s.d. | 960 | | 2.9 | 0.00705 | 485 | | 4.4 | 1.11 | 1375 | 0.000097 | 0.00410 | 0.15 | 0.008 |
| c.v. | 42.7% | | 25.0% | 0.7% | 33.7% | | 38.6% | 40.8% | 41.3% | 82.1% | 0.4% | 22.9% | 0.8% |

Table 2: D_E values and other data associated to the fitting of both SSE and EXP+LIN functions. Keys: s.d.=standard deviation; c.v.=coefficient of variation.

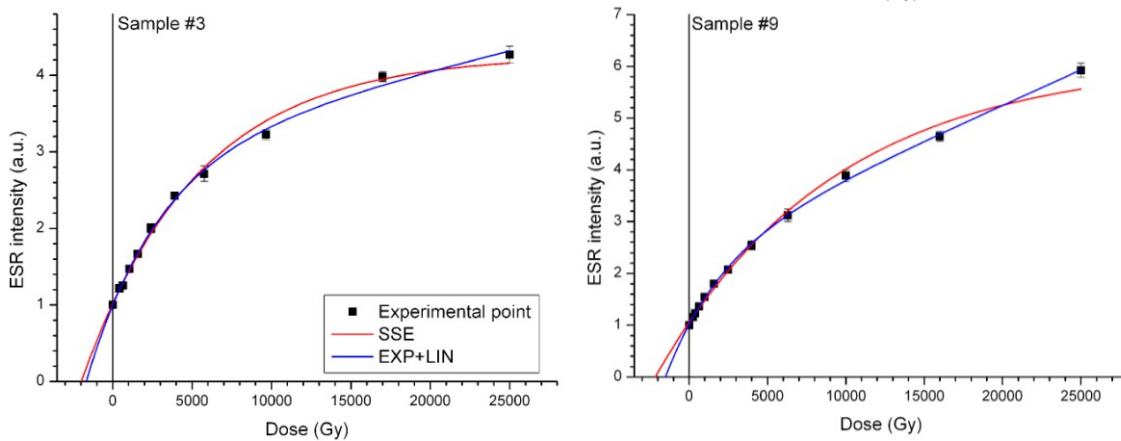


Figure 2: Dose response curves of samples #3 and #9, for which the SSE shows the best fitting of the data set ($Adjusted\ r^2 > 0.99$). Mean ESR intensities were calculated from repeated ESR measurements of each sample. Errors on the ESR intensities correspond to 1 standard deviation.

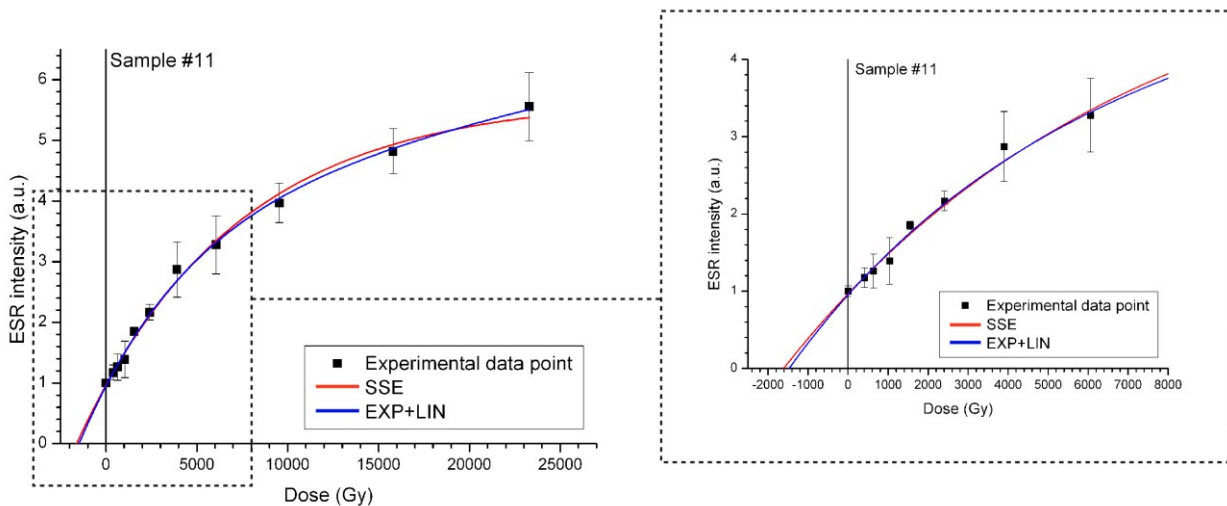


Figure 3: Example of a DRC with a high D_0 (6093 Gy): sample #11. Both SSE and EXP+LIN functions show close goodness of fit and D_E values. Mean ESR intensities were calculated from repeated ESR measurements of each sample. Errors on the ESR intensities correspond to 1 standard deviation.

DRCs are shown in Fig. 2. However, despite the apparent tight fit, one may observe that the experimental points are not particularly well fitted at doses higher than ~ 5 kGy. These observations suggest that the DRCs of the Al center in quartz cannot be correctly fitted with the SSE function.

Potential of the EXP+LIN function in comparison with the SSE

Two distinct domains can be identified in the DRCs shown in Fig. 1. First, the ESR signals increase quite rapidly with the dose in a few kGy, i.e. the natural ESR intensities are multiplied by a factor of ~ 3 -4 up from 0 to 4 kGy. Then the DRC grows more slowly at higher doses, with the ESR intensities multiplied by a factor of ~ 2 between 4 kGy and 25 kGy. Perhaps

the most striking observation is that there is almost no apparent saturation of the Al center at high doses (up to 40 kGy). This is in agreement with the data shown by Lin et al. (2006). The ESR signal grows almost linearly with the absorbed dose at irradiation doses in excess of ~ 4 -5 kGy (see also the DRCs shown in Duval et al. (2011) and Cordier et al. (2012)). Consequently, the hypothesis of a single component building the ESR signal, one of the basic assumption of the SSE function, is not valid. It seems that at least two components contribute to the ESR signal: the first saturates at low doses and the second shows no apparent saturation at high dose, with an almost linear behavior, justifying thus the use of an EXP+LIN function.

Like the SSE function, the EXP+LIN was fitted through the experimental data points of the 15 samples (see Table 2). Visually, the EXP+LIN function fits the data points much better than the SSE function (e.g. Fig. 1 and 2). This is confirmed by the adjusted r -square values: the EXP+LIN function provides a better fit than the SSE for 13 of 15 samples, even for those that were already well fitted with the SSE (#3 and #9). The two remaining samples (#11 and #12) show very close adjusted r -square values (Table 2). These were collected at the same cave site, Atapuerca Sima del Elefante, and show DRCs with the highest D_0 values of the data set (> 6 kGy). Consequently, it seems that a linear term could not be identified within the dose range used for the DRCs (Fig. 3). Here, at least a couple of additional irradiation steps at doses >25 kGy would be useful to identify the linear term and to reduce the large D_E errors ($>15\%$). In addition, the various ESR measurements of sample #11 show an especially quite poor precision, as indicated by the large errors in the ESR intensities (Fig. 3). This may explain why the adjusted r^2 values are < 0.99 for both functions, and suggest that the experimental data are not perfectly fitted for this specific sample. Basically, the best fits with the SSE are obtained for samples showing high D_0 values (e.g. samples #3, #9, #10, #11 and #12) but even there, the fitting with the EXP+LIN remains still very close or even better. In contrast, the DRCs from samples #5 and #6 have the lowest D_0 values of the data set, and the fitting of the SSE is totally inappropriate (adjusted $r^2 < 0.98$; e.g. Fig. 1).

Similarly to the previous results by Duval et al. (2009), D_E values calculated with the EXP+LIN function are systematically lower (on average by 37%) than those obtained with the SSE. The minimum deviations between the D_E derived from each function are around -8 % for the samples #11 and #12, i.e. those with the highest D_0 . The maximum deviation is obtained for samples with $D_0 < 2000$ Gy (samples #5 and #6), i.e. DRCs where the first exponential component saturates quite quickly and the second linear component takes over the former at relatively low dose values.

The impact of D_{max} on the fitting results for both functions is illustrated by Fig. 4 for samples #1 and #2 which had the largest number of data points (Table 1). Fig. 4A shows the evolution of the D_E values relative to the D_E values obtained at $D_{max}=40$ kGy. The application of the SSE function results in an almost linear increase of the D_E values: between $D_{max}=12$ kGy and $D_{max}=40$ kGy, the D_E value increases by a factor of ~ 1.4 - 1.6 for both samples. Such a strong correlation was one of the arguments against the use of the SSE function for tooth enamel

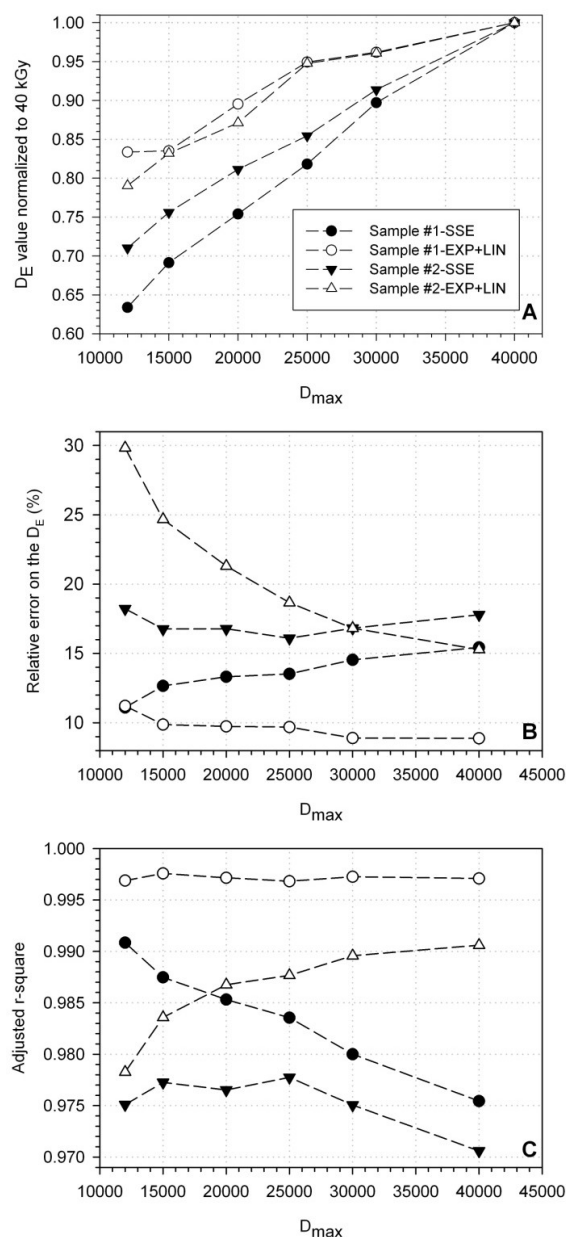


Figure 4: Influence of D_{max} on the fitting results: a couple of examples with samples #1 and #2. (A) Evolution of the D_E with D_{max} , from $D_{max}=12$ kGy to $D_{max}=40$ kGy. Current D_E values are normalized to the D_E obtained at $D_{max}=40$ kGy. (B) Evolution of the relative D_E error with D_{max} . (C) Evolution of the adjusted r -square with D_{max} .

samples (Duval et al., 2009; Chen et al., 1997). With the EXP+LIN function, D_E values have a similar increase between $D_{max}=12$ kGy and $D_{max}=25$ kGy. However, from $D_{max}=25$ kGy to $D_{max}=40$ kGy, the D_E values remain almost constant with only a slight increase of $<5\%$ over 15 kGy. Contrary to the SSE

function, the EXP+LIN function is much less dependent on the D_{max} , but it is critically dependent on having sufficient data points to define correctly the linear term at high doses. Similar trends were observed with other samples of the data set: the EXP+LIN D_E values remain almost constant when progressively removing the last 3-4 points, while SSE D_E values significantly decrease. Fig. 4B shows the evolution of the relative D_E errors with D_{max} . For the EXP+LIN, the errors are constantly decreasing when D_{max} increases. In contrast, D_E errors from SSE remain either constant or increase when adding additional dose steps, as a result of the fitting becoming more and more problematic. This trend is also widely observed on the other DRCs of the data set. Fig. 4C shows that the goodness of fit of the EXP+LIN is systematically better than that of the SSE for a given sample and a given D_{max} . In the case of the EXP+LIN function, the adjusted r^2 value increases or remains almost constant when the D_{max} increases, contrary to the SSE.

Reducing the error in the D_E with the EXP+LIN function

The application of the EXP+LIN function results in larger errors than using the SSE because four instead of three independent parameters are optimized (see samples #10, #11 and #12 which have similar EXP+LIN and SSE D_E values, Table 2). This can be addressed by increasing the number of dose steps. Usually one considers that 3-4 points per fitted parameter are necessary (Lyons, 1992). Consequently, between 12 and 16 dose steps should be used to fit the EXP+LIN function, making sure that there are at least 3 to 4 points to describe the almost linear behavior of the ESR signal at high doses (> 10 kGy).

In addition to selecting an appropriate dose range for the DRCs, the precision of the measurements can be increased through repeated ESR measurements of the same aliquot. ESR measurements of quartz are complex since several parameters have an influence on the data reproducibility. They may be experimental, such as the temperature of the room, cooling water or the cavity (the ESR signal of Al center is only visible at liquid nitrogen temperature). Other error sources are intrinsic to the sample, like its homogeneity (the standard analytical procedure is usually based on multiple grains and multiple aliquot measurements) or the angular dependence of the ESR signal in the ESR resonator. To ensure precision of the data, it is necessary to carry out a series of repeated measurements of a given aliquot after various rotations in the cavity and over several days. For example, each aliquot from samples #1 and #2 were measured 3 times after a $\sim 120^\circ$ rotation in the resonator over 4 and 3 days, respectively. Then, the

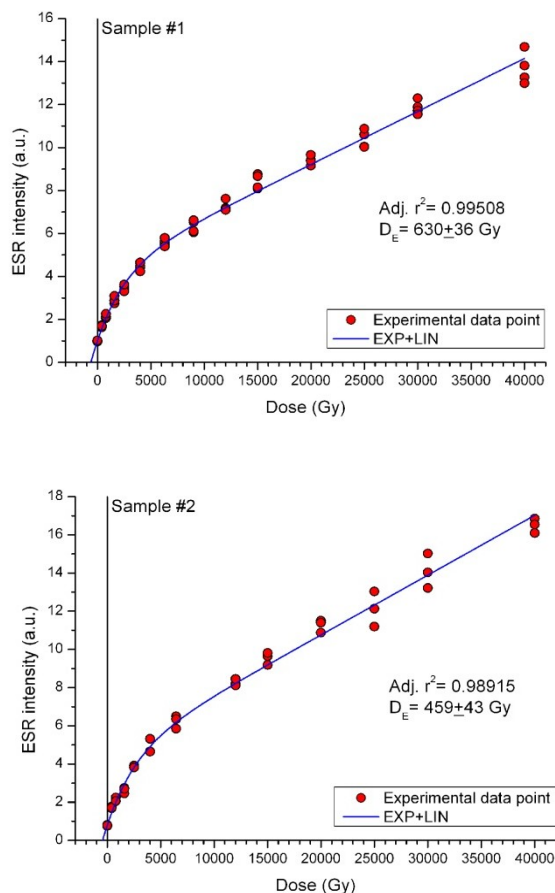


Figure 5: Influence of ESR data pooling on the D_E estimate (see comparison data from Table 2).

mean ESR intensities were extracted from each day of measurement and all these data may be plotted, making a data set of 51 and 39 data points for samples #1 and #2, respectively (Fig. 5). When comparing the results of the fitting with those derived from the initial fitting with one ESR data point for each aliquot, one may conclude that the impact on the D_E value is negligible ($\ll 1\%$, see Table 2), but the relative errors are much smaller by around 60% and 50%, respectively. These results are in agreement with the work by Grün and Brumby (1994) and Grün and Rhodes (1991, 1992) who showed that pooling of dose response points improve the random error in the D_E estimation.

Exploring a variation of the EXP+LIN function

As previously commented, the linear term may either correspond to the case where the second component saturates at such a high level that it may be approximated by a straight line (Walter et al., 1992), or where traps are generated during irradiation (Berger, 1990; Grün, 1990). With a linear term

| Sample number | EXP+LIN - Equation (3) | | | Equations (3) / (2) |
|---------------|------------------------|-------|------|----------------------|
| | D _E (Gy) | ± | % | D _E ratio |
| 1 | 729 | 70 | 9.6 | 1.16 |
| 2 | 545 | 91 | 16.6 | 1.19 |
| 3 | 1794 | 143 | 8.0 | 1.08 |
| 4 | 1891 | 201 | 10.6 | 1.11 |
| 5 | 1801 | 374 | 20.8 | 1.06 |
| 6 | 1173 | 89 | 7.6 | 1.16 |
| 7 | 1534 | 146 | 9.5 | 1.15 |
| 8 | 2116 | 248 | 11.7 | 1.15 |
| 9 | 1805 | 118 | 6.5 | 1.20 |
| 10 | 1631 | 211 | 12.9 | 1.07 |
| 11 | 1616 | 210 | 13.0 | 1.10 |
| 12 | 2385 | 330 | 13.8 | 1.09 |
| 13 | 1822 | 243 | 13.3 | 1.10 |
| 14 | 1032 | 81 | 7.8 | 1.11 |
| 15 | 2095 | 158 | 7.5 | 1.08 |
| Mean | | 11.30 | 1.12 | |
| s.d. | | 3.91 | 0.04 | |
| c.v. | | 34.7% | 4.0% | |

Table 3: D_E values obtained from the fitting of equation (3). Keys: s.d.=standard deviation; c.v.=coefficient of variation.

expressed by $m*(D+D_E)$, Equation (2) is basically supporting the first option. However, the impact of the second option on the D_E value may also be simply explored by slightly modifying the equation (2), as following:

$$I(D) = I_{sat} \left[1 - \exp\left(-\frac{(D+D_E)}{D_0}\right) \right] + mD \quad (3)$$

Table 3 shows the parameter values derived from the fitting of the equation (3). Basically, the equations (2) and (3) provide the same goodness of fit, similar relative errors ($11.4 \pm 4.4\%$ vs $11.3 \pm 3.9\%$ on average), D_0 and m values. The main differences lie in the modelled I_{sat} and the D_E values: using equation (3) systematically provides higher I_{sat} (+5% on average) and higher D_E values (+12% on average) than equation (2). However, it is worth noting that the D_E values obtained from each EXP+LIN function are consistent with unity at 1σ for 11 of 15 of the samples and at 2σ for all samples. D_E values derived from equation (3) are on average lower by about 26% than those obtained with the SSE.

The use of equation (3) would mean that the linear term is the specific result of high doses from laboratory irradiation, producing paramagnetic centers that would not be created in nature. However, because it is almost impossible to know whether the

first or the second option of the EXP+LIN should be preferred from a physical point of view, it seems reasonable for the time being to consider a mean D_E value extracted from the fitting of the two EXP+LIN functions (2) and (3) as the most reliable estimate of the true D_E value.

Conclusions

This work shows that the DRC of quartz is most appropriately fitted with an EXP+LIN function. This necessitates that the dose range for the DRC contains at least 2-3 data points at doses >10 kGy from which the linear section can be derived. Basically, if the linear part is not described, then the fitting procedure with the EXP+LIN becomes difficult, and sometimes impossible. This is the reason why it is recommended always to generate these high dose points, even when working with samples with D_E of a few hundreds of Grays, in order to minimize the impact of the D_{max} on the D_E value. The data set of this study (15 samples) shows the variety of DRC that may be encountered: the saturation dose D_0 varies by a factor of about 3.5 (from 1862 to 6493 Gy), indicating that some samples need to be more irradiated than others in order to get a good description of the linear term.

The preferential use of the EXP+LIN function to fit the experimental ESR data means that the ESR signal is driven by two main components, one dominating at low dose and the second dominating at high dose with an almost linear behaviour. This linear term may have two possible physical explanations, depending on the fitting equation selected. It could correspond to a component following a saturating exponential behaviour, but with such a large saturation dose that it can be approximated to a straight line. In that case, the paramagnetic center production is a continuing process. Such hypothesis is not so surprising, since the optical bleaching behaviour of the Al center also indicated the presence of two components (Voinchet et al., 2003), the first reducing the ESR intensity by about 50% within a few hours and the second further reducing the signal over several tens of days (Duval, 2008). Another hypothesis is that the linear term is only generated at high doses by laboratory irradiation, but not in nature. This would need to be further explored in the future. Given this uncertainty, the most reasonable option consists in considering a mean D_E value extracted from the fitting of both types of EXP+LIN functions, in order to encompass the two hypotheses.

On the other hand, the specificity of the D_E evaluation in ESR dating of quartz in comparison with other materials, or even with OSL dating, has to be considered. Since repeated ESR measurements of each aliquot are needed to ensure the data reproducibility, then all ESR intensities can be plotted and taken into account in the D_E assessment.

As soon as the data reproducibility is good, this would lead to a reduction of the error associated to the D_E value, in comparison with the plotting of a single set of mean ESR intensities. Such a procedure has been already suggested in the past by Grün et al (1992) and Grün and Brumby (1994), but the specificity of the ESR measurements of quartz makes now the pooling of ESR intensity necessary.

Finally, it is important to remind that even if the EXP+LIN function is more appropriate than the SSE to fit experimental data points of the Al center, this does not necessarily mean that the derived D_E values are accurate, i.e. the built-up of the natural ESR signal in the geological past may have been different to that reconstructed from additive dose points. It is obvious that additional experiments have to be carried out, such as comparing regeneration with additive DRCs on the same samples, and systematically comparing DRCs from geological successions, such as river terrace sequences where the quartz was most likely derived from the same source.

Acknowledgments

Verónica Guilarte performed some of the ESR measurements at the CENIEH. Thanks to Davinia Moreno, who kindly provided the DRCs data of the Madrid samples, and to all my colleagues, geologists, archaeologists or paleontologists for their help in the field. This study was partially sponsored by the projects CGL2010-16821 and CEN001B10-2 from the Spanish Ministry of Science and Innovation and the Junta de Castilla y León, respectively. Finally, I thank the reviewer, Rainer Grün, for helpful comments.

Supplementary Information for this article is available at www.aber.ac.uk/ancient-tl

References

Apers, D, Debuyst, R, de Canniere, P, Dejehet, F and Lombard, E (1981). A criticism of the dating by electronic paramagnetic resonance (ESR) of the stalagmite floors of the Caune de l'Arago at Tautavel. *Absolute Dating and Isotope Analyses in Prehistory—Methods and Limits*, Paris, CNRS.

Barabas, M, Mudelsee, M, Walther, R and Mangini, A (1992). Dose-response and thermal behaviour of the esr signal at $g = 2.0006$ in carbonates. *Quaternary Science Reviews* 11: 173-179.

Berger, GW (1990). Regression and error analysis for a saturating-exponential-plus-linear model. *Ancient TL* 8: 23-25.

Cordier, S, Harmand, D, Lauer, T, Voinchet, P, Bahain, J-J and Frechen, M (2012). Geochronological reconstruction of the Pleistocene evolution of the Sarre valley (France and Germany) using OSL and ESR dating techniques. *Geomorphology*. DOI: 10.1016/j.geomorph.2011.12.038.

Duval, M (2008). Evaluation du potentiel de la méthode de datation par Résonance de Spin Electronique (ESR) appliquée aux gisements du Pléistocène inférieur : étude des gisements d'Orce (bassin de Guadix-Baza, Espagne) et contribution à la connaissance des premiers peuplements de l'Europe. *Prehistory*. Paris, Muséum National d'Histoire Naturelle. PhD: 522.

Duval, M, Grün, R, Falguères, C, Bahain, JJ and Dolo, JM (2009). ESR dating of Lower Pleistocene fossil teeth: Limits of the single saturating exponential (SSE) function for the equivalent dose determination. *Radiation Measurements* 44: 477-482.

Duval, M, Moreno, D, Shao, Q, Voinchet, P and Falguères, C (2011). Datación por ESR del yacimiento arqueológico del Pleistoceno inferior de Vallparadís (Terrassa, Cataluña, España). *Trabajos de Prehistoria* 68: 7-24.

Fattahi, M, Stokes, S and Lamothe, M (2004). Red luminescence emission from potassium feldspars stimulated by infrared. *Ancient TL* 22: 35-44.

Goldberg, M, Mattern, PL, Lengweiler, K and Levy, PW (1973). Radiation induced coloring of Cherenkov counter glasses. *Nuclear Instruments and Methods* 108: 119-123.

Grün, R (1990). Dose Response of the Paramagnetic Centre at $g = 2.0007$ in Corals. *Ancient TL* 8: 20-22.

Grün, R and Brumby, S (1994). The assessment of errors in past radiation doses extrapolated from ESR/TL dose-response data. *Radiation Measurements* 23: 307-315.

Hoffmann, D, Woda, C and Mangini, A (2003). Equivalent dose determination in foraminifera: analytical description of the CO₂-signal dose-response curve. *Radiation Measurements* 37: 95-101.

Lee, H-K, Jack Rink, W and Schwarcz, HP (1997). Comparison of ESR signal dose-responses in modern and fossil tooth enamels. *Radiation Measurements* 27: 405-411.

Levy, PW (1985). Overview of nuclear radiation damage processes: phenomenological features of radiation damage in crystals and glasses. *SPIE* 541: 2-24.

Lin, M, Yin, G, Ding, Y, Cui, Y, Chen, K, Wu, C and Xu, L (2006). Reliability study on ESR dating

- of the aluminum center in quartz. *Radiation Measurements* 41: 1045-1049.
- Liu, C-R, Yin, G-M, Gao, L, Bahain, J-J, Li, J-P, Lin, M and Chen, S-M (2010). ESR dating of Pleistocene archaeological localities of the Nihewan Basin, North China – Preliminary results. *Quaternary Geochronology* 5: 385-390.
- Lyons, RG, Brennan, BJ and Hosking, PL (1992). Estimation of accumulated dose and its uncertainties: potential pitfalls in curve fitting. *Ancient TL* 10: 42-49.
- Rink, JW and Schwarcz, HP (1994). Dose response of ESR signals in tooth enamel. *Radiation Measurements* 23: 481-484.
- Rink, WJ, Bartoll, J, Schwarcz, HP, Shane, P and Bar-Yosef, O (2007). Testing the reliability of ESR dating of optically exposed buried quartz sediments. *Radiation Measurements* 42: 1618-1626.
- Voinchet, P, Falguères, C, Laurent, M, Toyoda, S, Bahain, JJ and Dolo, JM (2003). Artificial optical bleaching of the Aluminium center in quartz implications to ESR dating of sediments. *Quaternary Science Reviews* 22: 1335-1338.
- Voinchet, P, Falguères, C, Tissoux, H, Bahain, J-J, Despriée, J and Pirouelle, F (2007). ESR dating of fluvial quartz: Estimate of the minimal distance transport required for getting a maximum optical bleaching. *Quaternary Geochronology* 2: 363-366.
- Voinchet, P, Despriée, J, Tissoux, H, Falguères, C, Bahain, JJ, Gageonnet, R, Dépont, J and Dolo, JM (2010). ESR chronology of alluvial deposits and first human settlements of the Middle Loire Basin (Region Centre, France). *Quaternary Geochronology* 5: 381-384.
- Walther, R, Barabas, M and Mangini, A (1992). Basic ESR studies on recent corals. *Quaternary Science Reviews* 11: 191-196.
- Yokoyama, Y, Falgueres, C and Quaegebeur, JP (1985). ESR dating of quartz from quaternary sediments: First attempt. *Nuclear Tracks and Radiation Measurements* 10: 921-928.

Reviewer
R. Grün

Assessing the influence of the cavity temperature on the ESR signal of the Aluminum center in quartz grains extracted from sediment

M. Duval* and V. Guilarte Moreno

Centro nacional de investigación sobre la evolución humana (CENIEH), Paseo de Atapuerca s/n, 09002-Burgos, Spain

*corresponding author: mathieu.duval@cenieh.es (M.Duval)

(Received 25 June 2012; in final form 6 July 2012)

Abstract

In the present work, we briefly assess the potential of the Bruker Digital Temperature control system for ESR dosimetry/dating purpose and try to quantify the influence of the cavity temperature on the ESR signal of Aluminum center.

Our results also show that it is possible to reach a consistent level of repeatability in the ESR measurements with the Bruker Variable Temperature Unit (VTU) system, not only in terms of ESR intensities, but also for the equivalent dose (D_E) values. As expected, our results show a strong influence of the temperature on the ESR signal of Aluminum center. Given that dependence, it is recommended to apply some correction factors, especially when working around 90 K, in order to remove the systematic bias that may be induced by slight cavity temperature variations occurring during the measurement of a sample. However, despite the previous observations, there is no apparent impact of the temperature on the calculated D_E , whatever the cavity temperature between 90 and 110 K.

Introduction

One of the major specificities of ESR dating of Aluminium (Al) center in quartz is that ESR measurements have to be performed at low temperature, contrary to other materials like enamel or carbonates (e.g. Ikeya, 1993). Indeed, because of a very short spin-lattice relaxation time, the ESR signal of the Al center cannot be measured at room temperature. However, when the temperature lowers, the spin-lattice relaxation time becomes longer and the absorption lines are better resolved (Weeks, 1970).

A rapid overview of the bibliography indicates that the selected temperatures for the ESR measurements are quite variable (mainly from 77 K to 115 K), depending on the laboratories. Two systems are mainly used by the scientists dealing with ESR dating of Al center in quartz grains: the ESR measurements

are usually carried out using either a finger dewar filled with liquid nitrogen or a variable temperature control unit based on a nitrogen gas flow input (e.g., Lin et al., 2006; Liu and Grün, 2011; Tissoux et al., 2007; Voinchet et al., 2003). Both systems show strengths and weaknesses. On the one hand, the finger dewar allows ESR measurements at liquid nitrogen temperature (77 K), but its volume capacity is limited (usually <200 ml) and thus it has to be regularly filled by liquid nitrogen. This prevents continuous measurements over several hours. In addition, the bubbling of liquid nitrogen inside the dewar that may sometimes happen must be carefully controlled, because it can strongly affect the measured ESR signal. On the other hand, there are other systems that can automatically control and adjust the desired cavity temperature using a nitrogen gas flow input. They usually provide stable experimental conditions over a long time (several hours) and the target temperature may be chosen according to the needs of the users, but the temperature cannot go as low as that of the liquid nitrogen systems.

In the present paper, we briefly assess the potential of the Bruker Digital Temperature control system for dosimetric/dating purpose and we try to quantify the influence of the cavity temperature on the ESR signal of Aluminum center.

Experimental

ESR spectrometer

The ESR dating laboratory at the CENIEH (Burgos, Spain) is equipped with an EMXmicro 6/1 Bruker ESR spectrometer (Fig. 1) coupled to a standard rectangular ER 4102ST cavity. To ensure constant experimental conditions over time, the temperature of the water circulating in the magnet is controlled and stabilized at 18°C by a water-cooled Thermo Scientific NESLAB ThermoFlex 3500 chiller, and the temperature of the room is kept constant at 20°C by an air conditioning unit.



Figure 1: CENIEH's ESR spectrometry area: EMXmicro 6/1 Bruker ESR spectrometer connected to an ER4141VT Digital Temperature control system (with the flexible metal transfer line option).

Variable Temperature Unit (VTU)

The temperature of the ESR cavity (or ESR resonator) is regulated with a ER4141VT Digital Temperature control system, which is based on the following principles: the liquid nitrogen stored in a large dewar (25-50 L) is converted into gas by the evaporator and then goes through a metal transfer line to a quartz dewar insert that is placed in the cavity (Fig. 1). The temperature of the flowing gas is monitored with a thermocouple introduced in the dewar insert, close to the sample's position. The target temperature programmed by the user is reached and stabilized by the temperature controller, by combining the power of the liquid nitrogen evaporator and a heater (see further details in Barr, 1999). All the acquisition parameters, including the temperature of the cavity, are automatically saved with the ESR spectrum.

Initial tests of the Variable Temperature Unit (VTU) showed that our system could reach a minimum temperature of 85 K.

Stability of the system at low temperature

In ESR dosimetry/dating, it is really crucial to ensure constant experimental conditions, in order to eliminate, or at least minimize, the variations of the ESR signal that are induced by the system and to make sure that only the variations derived from the sample itself are recorded. In addition, the sample should be perfectly placed in the center of the cavity to ensure that all the aliquots of a sample are measured under identical conditions. Following our standard protocol for the Aluminium center, each aliquot of a given sample is measured 3 times after $\sim 120^\circ$ of rotation in the cavity, in order to take into account the angular dependence of the ESR signal. Usually, at least 1 hour is needed to complete the measurement of one sample formed by 10-12

aliquots. It is therefore crucial to make sure that the system (i.e., EMX spectrometer + VTU) is sufficiently stable to allow highly repeatable measurements over several hours at low temperature (<100 K).

Consequently, the stability of the system was assessed by leaving one aliquot in the cavity and by running continuous measurements at low temperature over a given time. Three examples of measurements at 85, 90 and 95 K are given in Fig. 2. The ESR intensities show a coefficient of variation (i.e., the ratio of the standard deviation to the mean) of $< 2\%$, i.e. of 0.8% at 95 K over 1 hour, 1.1% at 90 K over 3 hours and 1.5% at 85 K over 2 hours. Even though it seems that the lower the temperature is the least reproducible, this apparent pattern is not confirmed by supplementary measurements. Overall, repeated measurements do not show any systematic trend or significant drift in the ESR signal intensity with time. Consequently, it seems that the system is sufficiently stable to get repeatable measurements with less than 2% of variation. Perhaps our main recommendation when using the VTU, is to wait for a minimum period of 10 minutes once the system reaches the required temperature before starting the ESR measurements, in order to avoid the temperature and gas flow variations linked with the stabilization of the system.

Samples

We selected two samples from the palaeontological site of Villaroya (Rioja, Spain) (see Agustí and Oms, 2001 and references therein). Quartz grains were extracted following a standard procedure similar to that described in Voinchet et al. (2007). Gamma irradiations were performed with a Co-60 source at the following doses (dose rate=12.81 Gy/min): 250, 400, 630, 1000, 1600, 2500, 4000, 6300, 10000, 16000 and 25000 Gy.

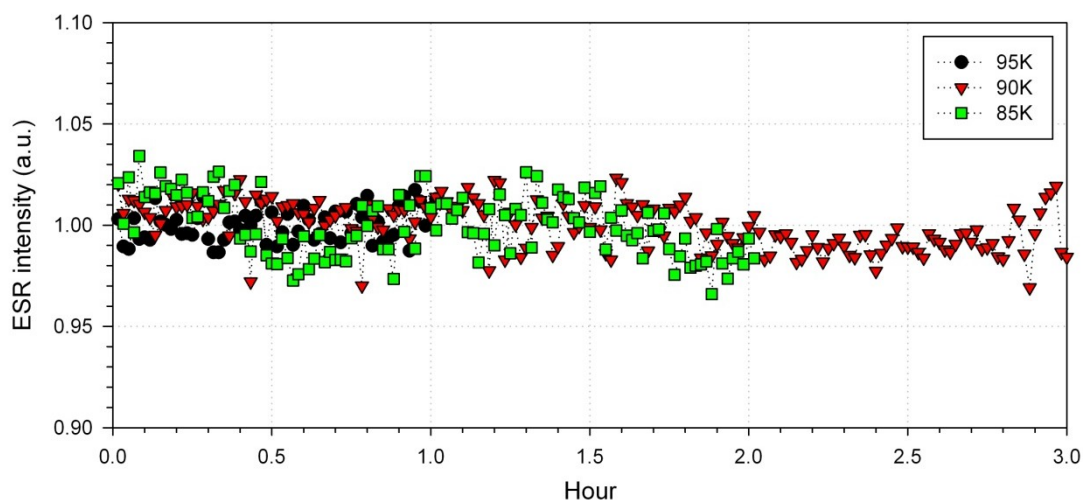


Figure 2: Evolution of the ESR intensity of three different samples with time. ESR intensities were normalized to the mean ESR intensity obtained for each sample.

Influence of the temperature on the ESR signal of the Al center in quartz

To evaluate the influence of the temperature on the ESR signal of the Al center in quartz, we ran a couple of wide range temperature sweeps from 90 to 300 K, with the two aliquots irradiated at 25 kGy from samples BUR1107 and BUR1108. Some examples of ESR spectra are shown in Figure 3. As expected, there is a clear correlation between the temperature of the cavity and the intensity of the ESR signal. Basically, the definition of the peaks and the intensity of the ESR signal of Al center are at a maximum when temperatures are at their lowest. Around 120 K, peaks almost disappear and only an envelope signal remains. Contrary to the ESR signals of Al- or Ti-center, the other ESR signals that are usually observed at room temperature (e.g., E', Germanium etc.) are becoming stronger and better defined as soon as the temperature increases (Fig. 3A). Further details about those paramagnetic centers may be found in Ikeya (1993).

ESR intensities of the Al signal were plotted versus the temperature for both aliquots (Fig. 3B). They show a similar evolution. There is first a strong temperature dependence between 89 and 93 K, with a decrease of 24% in intensity over the 4 K temperature range, i.e. -6%/K. Then, at higher temperature this influence is lower, with a value of -2%/K observed from 93 to 117 K. This correlation does not seem to be sample dependent, since similar trends were also observed using other quartz samples.

In order to get an overall description of the evolution of the ESR intensity of the Al signal with temperature, all the data were fitted with a polynomial function (5th order). Consequently, this equation can be used to correct the ESR intensity according to the temperature in the cavity for a given

ESR spectrum. Temperature correction factor values (normalized to T=90 K) are given in supplementary material. Consequently, given the strong correlation between ESR intensity and temperature ($r^2=0.99$), it is recommended to systematically correct the ESR intensity by a given factor, in order to remove the bias induced by the cavity temperature variations during the ESR measurement of a sample. This is especially crucial for temperatures less than 93 K. As an example, when working at 90 K, a variation of 0.1 K may induce a variation of about 1% in the ESR intensity. At 100 or 110 K, the same 1% of variation in the ESR intensity is caused by a variation of 0.7 and 0.9 K, respectively. For a given ESR spectrum, the temperature of the cavity is automatically saved with all the other acquisition parameters and can be simply obtained through the parameter list via the Bruker WinEPR Processing software. Therefore, each ESR measurement may be systematically associated to a given temperature value, and the ESR intensity may be corrected accordingly.

Influence of the temperature on the D_E values

We performed ESR measurements of the two samples BUR1107 and BUR1108 at 3 different temperatures (90, 100 and 110 K). Following the standard protocol described in Duval (2012), for a given temperature and a given sample: (i) each aliquot was measured 3 times after a $\sim 120^\circ$ rotation in the cavity in order to consider the angular dependence of the ESR signal, and (ii) 3 replicate measurements of the whole series of aliquots were carried out to check data repeatability. Consequently, a total of 9 ESR intensities were obtained for each aliquot. Each ESR intensity was corrected by the weight of the aliquot, the receiver gain and the cavity temperature and then normalized by the mean

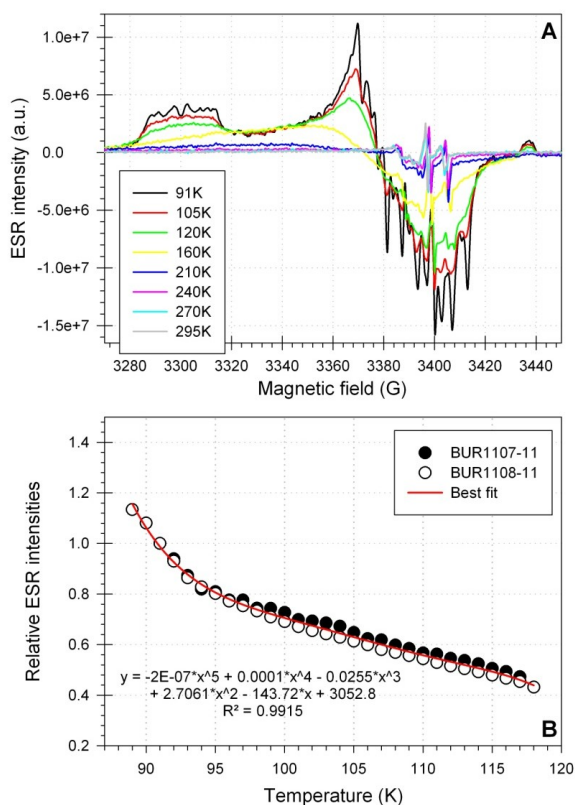


Figure 3: Influence of the temperature on the ESR signal of Al center in quartz. (A): Evolution of the ESR signal of the sample BUR1108 ($D=25$ kGy) from $T=91$ K to $T=295$ K (room temperature). Acquisition parameters: 10 mW microwave power, 2048 points resolution, 100 mT sweep width, 100 kHz modulation frequency, 0.05 mT modulation amplitude, 30 ms conversion time, 10 ms time constant and 3 scans. (B): Evolution of the ESR intensities (normalized for $T=91$ K) according to the temperature. The ESR intensity of the Al signal was extracted from peak-to-peak amplitude measurements between the top of the first peak ($g=2.0185$) and the bottom of the 16th peak ($g=1.9928$) (Toyoda and Falguères, 2003).

intensity of the natural aliquot for a given sample, in order to get comparable data from one series of measurements to another (ESR data are available in Supplementary Information). For each sample, the D_E values were calculated by pooling the 9 normalized ESR intensities and fitting an exponential+linear function through the experimental data points (see Duval, 2012), using Microcal OriginPro 8.5 software. Data were weighted by $1/I^2$.

For a given temperature and a given sample, ESR intensities show good repeatability, with an average coefficient of variation ranging from 1.2 to 1.8% (supplementary information). For a given sample, no

apparent correlation is observed between the ESR intensity variability and the temperature.

Table 1 shows the D_E calculated for each target temperature. Dose response curves are given in Fig. 4. All the D_E values show a deviation of less than 5% for a given sample. For BUR1107, the D_E value obtained at 90 K (2531 ± 122 Gy) is slightly higher, by $\sim 5\%$, than those obtained at 100 K and 110 K (2415 ± 108 Gy and 2415 ± 131 Gy, respectively). For BUR1108, the deviation is even smaller ($< 3\%$) and D_E values range from 1996 ± 78 (100 K) to 2057 ± 69 Gy (110 K). Nevertheless, it is worth noting that all the values are consistent at $\pm 1\sigma$, thus indicating that there is no apparent impact of the temperature on the D_E .

Temperatures registered for each ESR spectrum are very stable during the measurement of all the aliquots of a given sample, but also over the series of 3 full measurements. In addition, we also observed that temperature variations may be minimized if a pause before each measurement is included in the protocol, to ensure that the temperature is stabilized and remains constant at, at least, ± 0.3 K from one measurement to another. Depending on the series, the amplitude of temperature variations over a given series usually ranges from 0.1 to 0.2 K, though a higher value (0.4 K) may be sometimes be observed (see supplementary information). The influence of these slight temperature variations on the ESR intensities may be then simply removed by using the corresponding correction factors. However, as mentioned above, this temperature variability is less crucial for higher temperature (110 K) measurements, since the ESR intensity remains more or less stable over ~ 0.9 K.

In addition, it is also worth taking into account some practical considerations when working at low temperatures. We observed that between each aliquot the system needs much more time to stabilize the temperature around 110 K (~ 1 min) than at 90 K (a few seconds), requiring then a longer measurement time for a given sample comprising 10-12 aliquots (around 15 minutes more). This may seem a priori somewhat counterintuitive, since it is easier for the system to initially drop in temperature and stabilize at 110 K than at 90 K. However, this may be simply explained as following: at 110 K, when replacing one tube with another, the environmental conditions in the cavity quickly change once the tube is out, and the temperature drops by a few K, because the power of the evaporator and the heater remain constant for a few seconds. Then, the system tries to stabilize the temperature at the desired value, by adjusting the heater power, and induces some temperature oscillations around the target temperature value before stabilization. However, at 90 K, the evaporator

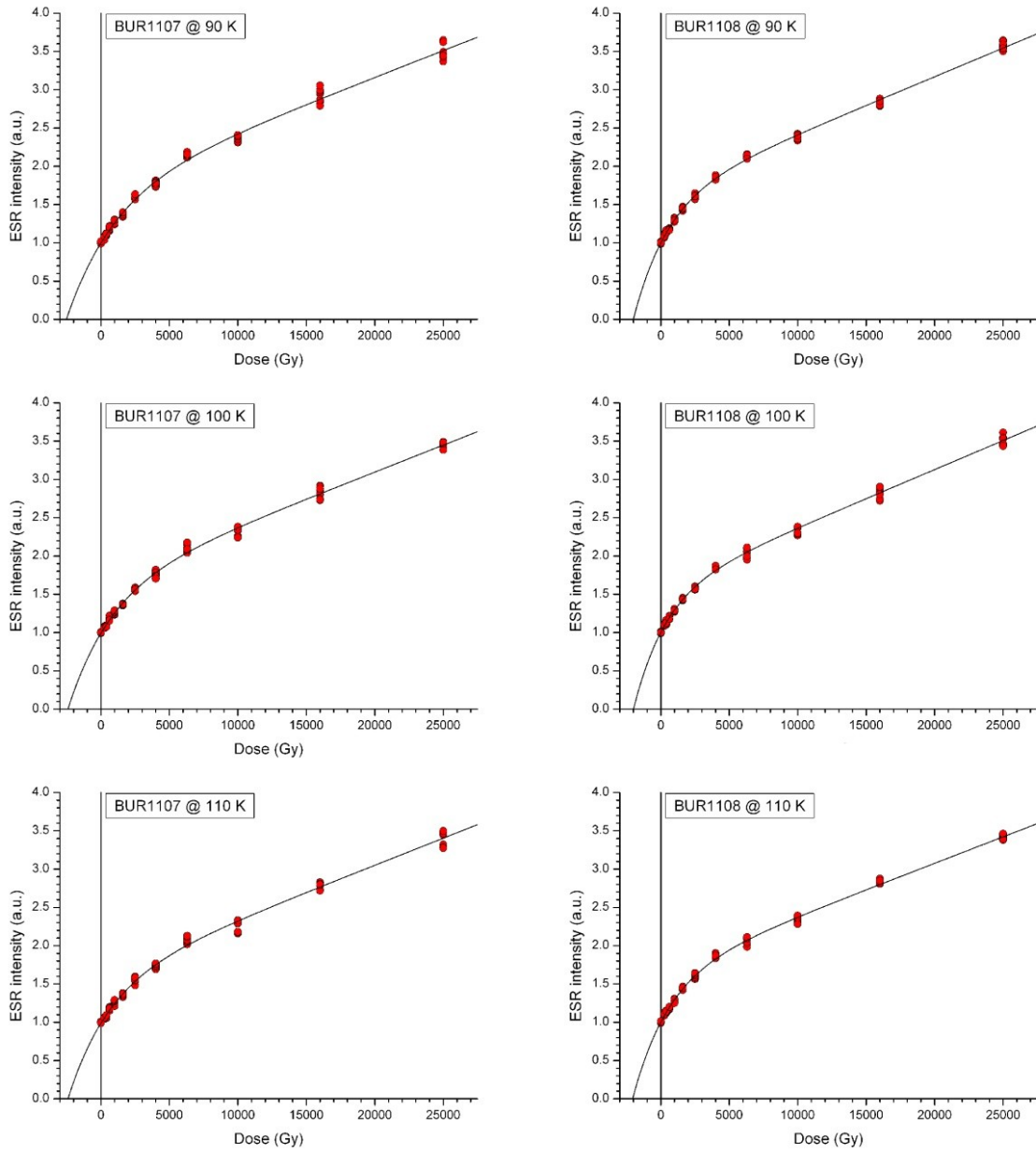


Figure 4: Dose response curves obtained for samples BUR1107 and BUR1108 at 90, 100 and 110 K.

| | T=90 K | T=100 K | T= 110 K | Ratios | | |
|---------|-------------|-------------|-------------|--------|------|------|
| | 1 | 2 | 3 | 2/1 | 3/1 | 3/2 |
| BUR1107 | 2531±122 Gy | 2415±108 Gy | 2415±131 Gy | 0.95 | 0.95 | 1.00 |
| BUR1108 | 2007±68 Gy | 1996±78 Gy | 2057±69 Gy | 0.99 | 1.02 | 1.03 |

Table 1: D_E values derived from ESR measurements performed at 90, 100 and 110 K.

power is at 100% and the system is very close to the minimum possible temperature, so that any changes of tube only produce a small variation of the cavity temperature (1-2 K max.). It is thus easier and faster for the system to get stabilized at 90 K after every change of tube in the cavity.

Conclusions

Our results show that it is possible to reach a consistent level of measurement repeatability with the Bruker VTU. This system offers the possibility of working at any temperature from room temperature to ~85 K, and shows several points of interest: (i) it provides stable experimental conditions over several hours (<1.5% of variation) for temperatures <95 K, (ii) the temperature is registered for each measurement, allowing some further corrections for each single spectrum, (iii) the temperature remains stable during the measurements of all aliquots of a given sample (<0.4 K of amplitude), (iv) the ESR intensities of a given aliquot are very reproducible (<2% of variation) from one measurement to another.

As expected, our results show the strong influence of the temperature on the ESR signal of the Al center. The signal and the peaks are well resolved around 90 K, while at 110 K the peaks cannot be identified and only an envelope signal of the Al center can be observed. Given the dependence of the ESR intensity on the temperature, it is recommended to apply correction factors, especially when working around 90 K, in order to remove the systematic bias that may be induced by slight temperature variations during the measurement of a sample. At this temperature, a variation of 0.1 K may induce 1% of variation on the ESR signal intensity.

However, despite the previous observations, there is no apparent impact of the temperature on the calculated D_E , since all the values are consistent at $\pm 1\sigma$, whatever the temperature between 90 and 110 K. Nevertheless, it is worth considering that working at 110 K may create some additional problems. Indeed, since the ESR signal is not well resolved at that temperature, the peak-to-peak measurement may be sometimes quite complicated and inaccurate. In addition, between each aliquot the system needs much more time to stabilize the temperature around 110 K than at 90 K, requiring then a longer measurement time for a given sample.

Acknowledgments

This study was partially sponsored by the projects CGL2010-16821 and CEN001B10-2 from the Spanish Ministry of Science and Innovation and the Junta de Castilla y León, respectively. Thanks to Alfonso Benito Calvo and Arsenio Muñoz for their help during the sampling.

Supplementary Information for this article is available at www.aber.ac.uk/ancient-tl

References

- Agusí, J. and Oms, O. (2001). On the age of the last hipparionine faunas in western Europe. *Comptes Rendus de l'Académie des Sciences - Series IIA - Earth and Planetary Science* 332(4): 291-297.
- Barr, D. (1999). EMX User's Guide for the ER 4131VT Variable Temperature Accessory. Manual Version 1.0. Bruker Instruments, Inc.
- Duval, M. (2012) Dose response curve of the ESR signal of Aluminum center in quartz grains extracted from sediment. *Ancient TL* 30: 1-9
- Ikeya, M (1993). *New Applications of Electron Spin Resonance Dating, Dosimetry and Microscopy*. Singapore, World Scientific.
- Lin, M, Yin, G, Ding, Y, Cui, Y, Chen, K, Wu, C and Xu, L (2006). Reliability study on ESR dating of the aluminum center in quartz. *Radiation Measurements* 41: 1045-1049.
- Liu, C-R and Grün, R (2011). Fluvio-mechanical resetting of the Al and Ti centres in quartz. *Radiation Measurements* 46: 1038-1042.
- Tissoux, H, Falguères, C, Voinchet, P, Toyoda, S, Bahain, JJ and Despriée, J (2007). Potential use of Ti-center in ESR dating of fluvial sediment. *Quaternary Geochronology* 2: 367-372.
- Toyoda, S and Falguères, C (2003). The method to represent the ESR signal intensity of the aluminium hole center in quartz for the purpose of dating. *Advances in ESR Applications* 20: 7-10.
- Voinchet, P, Falguères, C, Laurent, M, Toyoda, S, Bahain, JJ and Dolo, JM (2003). Artificial optical bleaching of the Aluminium center in quartz implications to ESR dating of sediments. *Quaternary Science Reviews* 22: 1335-1338.
- Voinchet, P, Falguères, C, Tissoux, H, Bahain, J-J, Despriée, J and Pirouelle, F (2007). ESR dating of fluvial quartz: Estimate of the minimal distance transport required for getting a maximum optical bleaching. *Quaternary Geochronology* 2: 363-366.
- Weeks, RA (1970). Paramagnetic Resonance and Optical Absorption in Gamma-Ray Irradiated Alpha Quartz: The "Al" Center. *Journal of The American Ceramic Society* 53: 176-179.

Reviewer

E.J. Rhodes

A novel beta source design for uniform irradiation in dosimetric applications

D.Richter^{1,3,*}, R. Pintaske^{2,1}, K. Dornich¹, M. Krbetscheck^{†4,1}

¹ Freiberg Instruments GmbH, Am St. Niclas Schacht 13, 09599 Freiberg, Germany

² Pintaske consulting, Annaberger Strasse 240, 09125 Chemnitz, Germany

³ Geographisches Institut, LS Geomorphologie, Universität Bayreuth, Universitätsstr. 30, 95447 Bayreuth, Germany

⁴ Senckenberg Museum of Mineralogy and Geology Dresden, Luminescence Section, c/o Inst. Appl. Physics, TU Freiberg, Leipziger Str. 23, 09596 Freiberg, Germany

* corresponding author: DR Daniel.Richter@freiberginstruments.com

(Received 21 October 2012; in final form 8 December 2012)

Abstract

A novel beta radiation source, specifically developed for the lexsyg luminescence system, was studied by radiochromic film. A circular arrangement of miniaturized sources creates a homogeneous radiation field, with a variation of 2% of radiation dose across the central 8 mm diameter of the target irradiated. While this arrangement is very efficient to achieve homogeneous irradiation, it also allows the simultaneous luminescence detection of radio-fluorescence through the hole in the source body. The geometry of the irradiation set-up, in particular the material, the size and the shape of the substrate carrier affect the actual dose distribution and dose rate at the target site to a larger extent than any inhomogeneity of this source itself.

Introduction

In dosimetric applications the uniformity of laboratory irradiation is crucial. While this can be easily achieved by photon irradiation with rather homogeneous irradiation fields (e.g. by ¹³⁷Cs or ⁶⁰Co γ -sources), such are often not available, or simply not feasible, for example in the application of the single aliquot regeneration (SAR) protocol to reconstruct the response of material to radiation. Radiation fields of sources used in luminescence dating applications are mostly reported with concentrically decreasing dose-rates away from the centre of the target (e.g. Spooner and Allsop, 2000). For typical diameters of 6 - 10 mm the radiation field of ⁹⁰Sr/⁹⁰Y beta sources has been reported to vary spatially at least between 3% for a distance of 9.75 mm from a 4 cm² active area (Sanderson & Chambers, 1985), 10% for a 1 cm² active area (e.g. Bailiff, 1980; Veronese et al., 2007) and 30-40% (Spooner & Allsop, 2000). For larger areas of interest (8 - 10 mm diameter) the field inhomogeneity was found to vary sometimes by a

factor of two and additionally sometimes shows a skewed concentric pattern in the radiation field (e.g. Ballarini et al., 2006), if the widely used ⁹⁰Sr/⁹⁰Y beta sources (SIF and SIP type) are considered.

Larger distances between the source and sample provide more homogeneous irradiation fields, as do sources with active surfaces which are larger than the target surface (Aitken, 1985). Furthermore a large distance also reduces the effects of the dependence on distance of approximately 10% mm⁻¹ (Aitken, 1985).

Inhomogeneities of irradiation can be reduced by moving the sample in a small circle during irradiation (e.g. the "jitter" facility of the Littlemore 9022A irradiator), or by moving the grains constantly during irradiation on a vibrating plate (Valladas and Valladas, 1982).

As a consequence of inhomogeneities of the artificial radiation field in luminescence dating the individual grains on multiple grain sample carriers will receive different individual doses, requiring the calibration of each individual grain position in single grain applications (e.g. Veronese et al., 2007), which is a tedious and error-prone procedure. Any effects of calibration sample dependencies, sample translucency, etc. will be enhanced by an inhomogeneous radiation field, which could be responsible for several second order effects and artefacts of the interaction between the sensitivity distribution within samples and the artificial radiation field. We here consider an irradiation as homogeneous if the absorbed dose variation is 3% or better for the area of interest, which is lower than the associated uncertainty for β -source calibration (Aitken 1985).

The homogeneity of an irradiation with a β -emitter is a function of source uniformity, source diameter, distance of active surface to area/volume to be

irradiated, shape, and size of the latter, as well as any material close enough to be included in any bremsstrahlung and backscatter effects (e.g. source housing, target substrate, etc.). These variables also determine the relationship between source strength and dose rate at the sample. From a luminescence dating application point of view, the former should have a low surface activity to minimise radiation safety concerns, while the latter should be large in order to maximise efficient use of luminescence readers and increase laboratory throughput, especially with respect to the SAR protocol. The desire to increase dose rates from sources of modest activity has led to closer coupling between source and sample, resulting in an inhomogeneous irradiation field, and potentially exacerbating the effects of heterogeneity of the activity distribution across radiation source with small active areas.

The main component of the resulting radiation field of a beta source encased in a housing is direct beta radiation from the source. Depending on the design of the source, the source holder etc., the radiation field will be significantly affected by scattered beta radiation and bremsstrahlung as well. The latter is produced by beta interaction within the material of the source, its housing, and shielding (Liritzis and Galloway, 1990). Furthermore, the material to be irradiated and its substrate as well as any material within the range of beta or bremsstrahlung also influence the radiation field (e.g. Ingram et al., 2002) and are therefore important parameters to be considered if homogeneous irradiation is required.

In developing the lexsyg luminescence measurement system one of the design requirements was to allow easy and direct radiofluorescence (RF) measurement. This is normally achieved with a source placed underneath the sample (e.g. Erfurt et al., 2003), which limits other uses of the source; or with a source above the sample and luminescence measured via a light guide (e.g. Bøtter-Jensen et al., 2003; Lapp et al., 2012), with a potentially significant loss in efficiency. An alternative approach is to use a ring source design with an opening for direct light collection to a detector, which has the added advantage of providing a more uniform radiation field than could be achieved using a conventional disc source. As indicated above, homogeneous irradiation is highly desirable in dosimetric and dating applications, where secondary effects of non-uniformity may be hard to quantify. It is also important in developments in single grain or surface area luminescence detection. The purpose of the current paper is to present data on the radiation characteristics of a novel beta radiation source developed for the lexsyg reader, and to discuss parameters affecting the radiation field quality while applied to luminescence measurements. The radiation

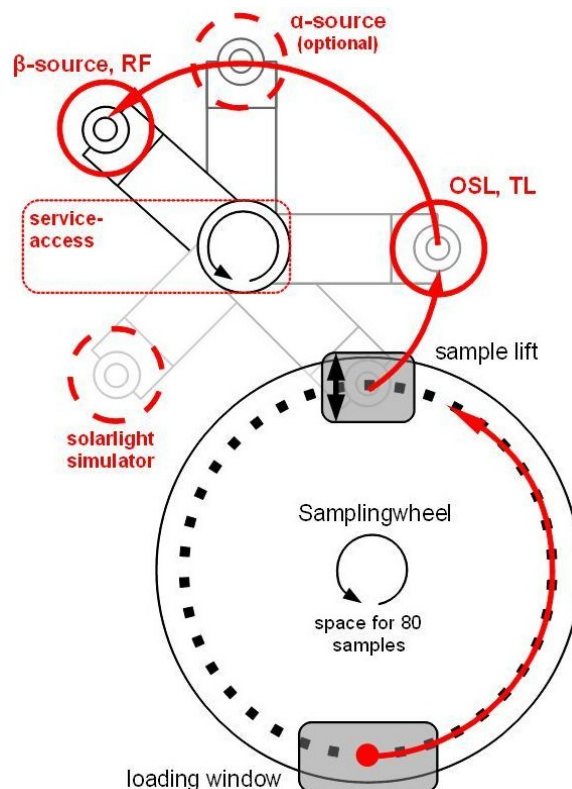


Figure 1: Schematic setup of a lexsyg system, where the sample wheel is separated from the measurement/stimulation or irradiation.

field produced by the new source has been measured using radiochromic films and dependency on the geometry of surrounding materials in the reader, and the sample substrates of the irradiated material have been investigated for a fixed source to sample distance.

The lexsyg luminescence system

In the modular lexsyg luminescence system the samples are placed in a circular sample holder accommodating 80 positions. During the measurement sequence the sample to be analysed is moved from the sample wheel to separate irradiation positions and measurement stations as required using a pick-and-place system, illustrated as an arrow in Fig. 1. There are no other samples in the vicinity of the sources used for irradiation, and the irradiation takes place away from illumination sources used in luminescence measurements. Therefore, light exposure of other sample aliquots is absent and radiation cross talk is negligible due to the large separation between the radiation source(s) and the sampling wheel. However, because the sample disc/cup stays on the heating plate all the time during

standard (i.e. SAR) measurement cycles and is neither lifted nor itself moved, neither the grains nor the sample carrier move their (relative) positions on the disc/cup or the heating plate. This has been verified for 10 times of movements between source and measurement positions. In fact, it does not appear to be necessary for the grains to be fixed by silicone oil.

A new β -source

In order to achieve direct radiation while measuring RF and to obtain a homogenous radiation field which also would allow spatial luminescence analysis without error prone differential area calibration, a new β -source has been developed for the lexsy system.

Design of the $^{90}\text{Sr}/^{90}\text{Y}$ -source

The beta source is intended for the direct irradiation of samples for RF as well as for TL/OSL applications and therefore the design in the form of a ring is most feasible, with a hole in the centre of the source body (activity carrier). This allows efficient, simultaneous light detection during RF. The design of the beta radiation source features a circular arrangement of miniaturized, sealed beta sources (Fig. 2). In order to create a homogeneous radiation field at the target site (sample, aliquot), each individual source is pre-selected according to its activity (<5% variation), before being mounted into a circular groove (14 mm diameter) of a stainless-steel source body. Thus, a circular activity distribution is formed. A stainless steel foil is micro-laser welded to the source body to fix the miniaturized sources in the groove. The field characteristics at irradiation distance are mainly governed by the diameter of the ring of activity, the material of the source body, the shape of the groove and the thickness of the cover foil.

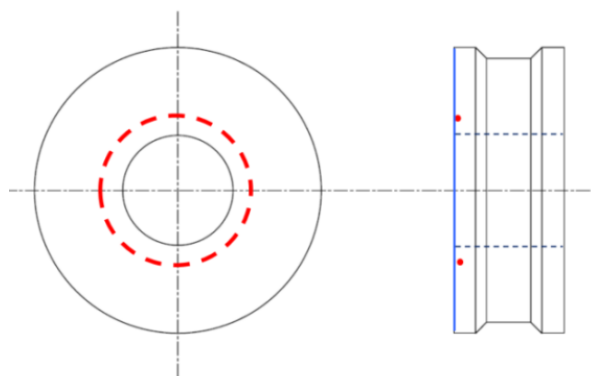


Figure 2: Schematic drawing of the source: dotted line – circular arrangement of miniaturized sources forming an active “wire”, bold line – radiation window (stainless steel foil)

Characterization of the radiation field of the $^{90}\text{Sr}/^{90}\text{Y}$ -source

The radiation field at the target site was investigated using radiochromic, self-developing films (GafChromic film type HD-810 from ISP, Inc.). This type of radiation detector provides high-resolution, two-dimensional information on the dose distribution. The purpose here is a qualitative determination of the spatial variation of absorbed dose. These are investigated for dependencies on source as well as sample carrier geometry.

The optical density of the irradiated films was determined by an LED scanner NIKON CoolScan IV ED at 300 dpi resolution. Calibration in terms of soft tissue equivalent dose was achieved through a NIST calibrated reference β -source (Sr-90, type QQ251). Note that the current investigation primarily deals with radiation field uniformity rather than dose rate, thus the tissue equivalent dose rate has been used to gather this information. The field distributions and profiles are shown as normalized absorbed doses.

Experimental setup

Due to the limited size of the lexsy sample carrier (heating plate) it was considered to be too difficult to reproduce the entire area occupied by samples with radiochromic films placed within the lexsy luminescence reader. Thus, the geometry of the reader was mimicked as closely as possible in a special experimental set up. Challenges here are the necessity to hold the films planar and stabilize a film of a size large enough in order to guarantee enough space between the unusable area at the film edge (1-2 mm rim) and the area of interest (sample area size of ~8 mm diameter). Furthermore, the geometry and material of sample targets/holders have an influence on the dose distribution. Additionally, sample geometries obviously can have effects as well, but are not the purpose of this study and are therefore not considered here.

Experiments were repeated at least three times with exposure periods between 50 and 70 minutes, always providing the same results and representative figures (Fig. 3-5) are shown for all experiments.

Three different experimental settings were employed, while keeping the source to heating plate distance of 7.7 mm constant. First, the uniformity of irradiation was measured in a 'free in air' experiment where all materials needed to hold in place the radioactive source were minimized and the film placed on a wide acrylic glass substrate to avoid the influence of edge effects from the backscatter caused by the substrate and the source holder. This allows the evaluation of the dose distribution created by the source exclusively, with the least influencing geometry factors (Fig. 3A) and provides insight in the variation exclusively caused by the geometry of the

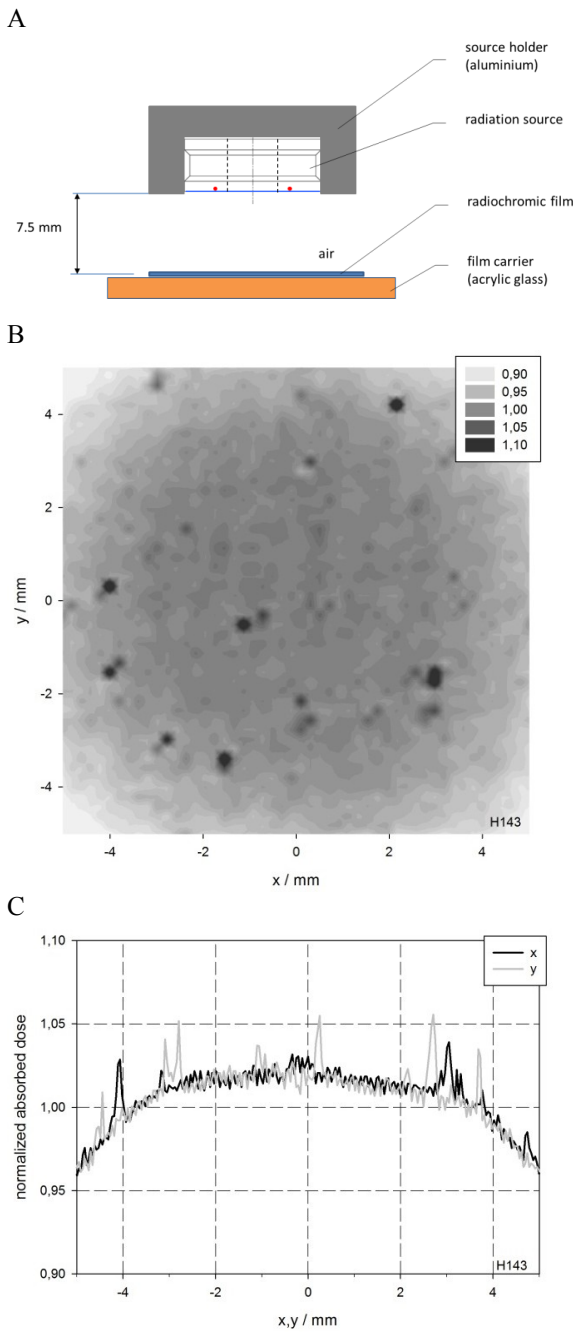


Figure 3: 'Free in air' experiment with minimized influence of other materials. (A) geometry with film on a large area substrate and radioactive source mounted with minimized material, where the source holder isn't shown for the sake of simplicity (not to scale); (B) contour plot of normalized spatial dose distribution for the irradiated area within the limits of the usable area of the film; (C) normalized absorbed doses for two profiles (x and y) perpendicular to each other. The actual range of interest is between -4 and +4 mm, which corresponds to the available area of 8 mm inner diameter of cups, intended for use in the lexsys systems.

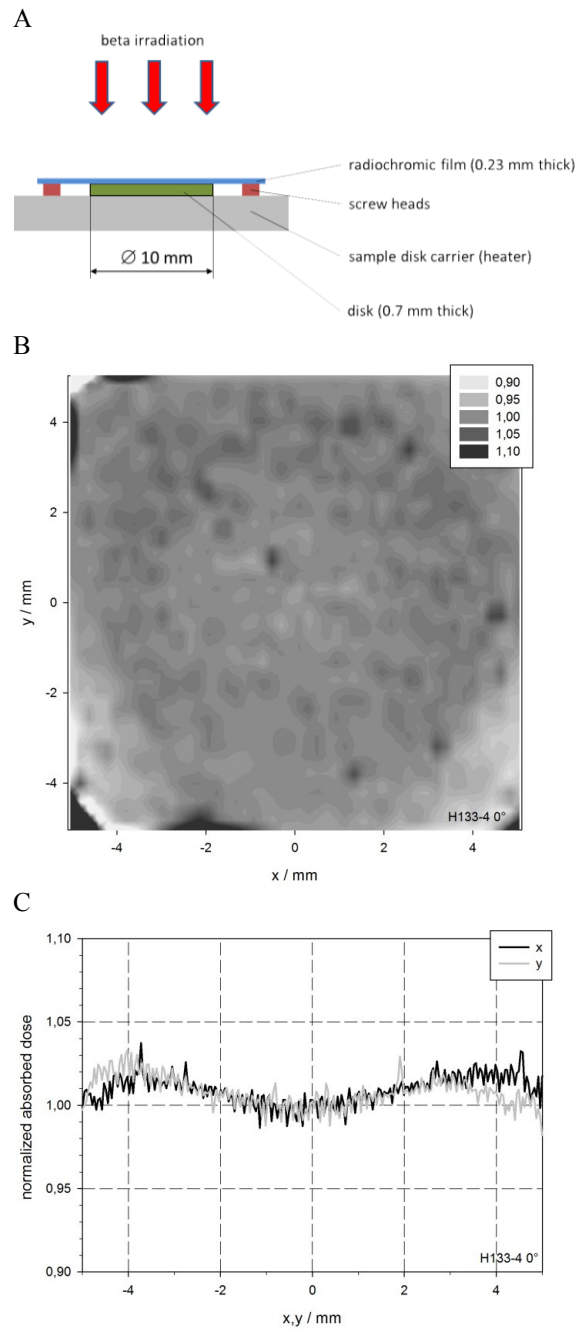


Figure 4: Experimental setup to mimic the irradiation of a sample on a flat disc in a lexsys reader. The geometry of the source mounting and film placement was identical to the actual situation in a reader by using e.g. an original heater plate on arm. (A) Geometry; (B) contour plot of normalised absorbed dose; (C) normalized absorbed doses for two profiles (for more details see Fig. 3 caption).

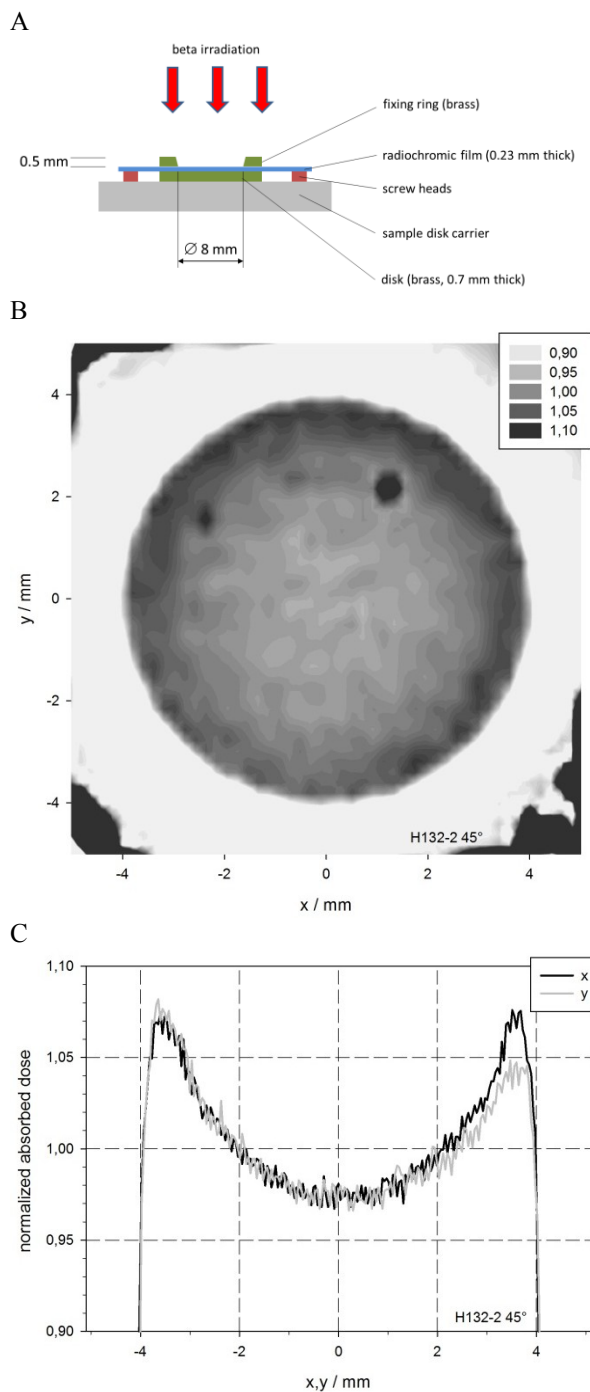


Figure 5: Experimental setup to mimic the irradiation of a cup in a lexsyg reader. The geometry of the source mounting and film placement was identical to the actual situation in a reader by using e.g. an original heating plate mounted on an original arm, but a ring was placed on top of the film with a disc underneath to mimic the rim of a cup. (A) geometry; (B) contour plot of normalised absorbed dose; (C) normalized absorbed doses for two profiles (for more details see Fig. 3 caption).

source in its housing. However, the actual irradiation in a measurement system takes place in a more complex geometry, and includes backscatter effects which affect the radiation field.

The laboratory setup to mimic the geometry in the lexsyg system allows reproducible experiments under optimized conditions, with the film placed on a heating plate mounted on an arm as used within a system. The film here takes the place of a sample on a carrier substrate, while the radioactive source in its housing is mounted the same way as in the lexsyg system, but easy access is possible. In one of such experiments the film is placed on a disc which is only slightly thicker than what is commonly used as sample carrier (Fig. 4A), but thick enough to ensure backscatter saturation.

In the other experiment a ring of the outer diameter of such a disc and 0.5 mm thickness is additionally placed on top of the film to mimic a 'cup' as sample carrier (Fig. 5A) and investigate the influence of the form of the sample carrier on the radiation field. It is not possible to perform reliable measurements with a film within an actual sample 'cup' because the areas close to the edges of a film is unusable for analysis. The rim of a cup limits the size of the film which can be placed and thus only an area smaller than the actual area of interest of the radiation field would be available.

Furthermore, measurements were performed for four different substrate materials (brass, aluminium, nickel and two different stainless steel) placed as 10 mm diameter discs of 1.0 mm thickness each underneath the film (film is thus at sample position).

Results of film measurements

The results are presented as contour plots (B of Figs. 3-5) of the relative absorbed dose for the irradiated area within the limits of the usable area of the film. The actual variation can be better visualized as normalized absorbed doses for two profiles (x and y) perpendicular to each other (C of Figs. 3-5). Note the limited scale of only 0.9 - 1.1 of the normalized dose for all graphs. Even though the practical range of interest is between -4 and +4 mm from the centre, which is corresponding to the available area of 8 mm diameter within the cup/discs used in the lexsyg systems, a wider x-y range is displayed for informative purposes. Local inhomogeneities of the film material caused by handling of those unusually small film pieces are responsible for the peaks/spikes observable especially in the dose profiles. Such apparent 'hot spots' are artefacts of the radiochromic film and do not correspond to the groove which holds the sources. Furthermore, slight asymmetries, which are likely caused by film positioning (film not lying perfectly flat on the substrate material), are noticeable.

All distributions show either a maximum or a minimum of the absorbed dose at the centre of the irradiation field. When the film is placed on a material of a size much larger than the irradiated area, a maximum value in the centre is observed (Fig. 3C). This contrasts with a minimum in absorbed dose if the edge of the substrate is close to the area of irradiation (Fig. 4C).

In a "basic" geometry, i.e., the source simply positioned over a film while minimizing the amount of surrounding material to minimize (backscatter) effects, the variation in absorbed dose is about 2% over the area of interest of 8 mm diameter and about 6% for 10 mm diameter (Fig. 3C). An even wider homogeneous irradiation field appears to be obtainable when a tube of a diameter slightly larger than the active area is located underneath the source (not shown), which appears to slightly increase Bremsstrahlung and thus promotes homogeneity of the radiation field. While placing such a tube is certainly not feasible in automated irradiation, it might provide an opportunity for further developments in irradiation fields.

For a geometry identical to the one in a lexyg luminescence reader and a flat disc of 10 mm diameter as substrate, the variation is about 3% over the entire area with a small edge effect noticeable (Fig. 4C). For the identical set up and the geometry of a 'cup' with a ring placed on top the film, the edge effect becomes rather pronounced, leading to a variability of 10% of the area of 8 mm diameter where sample material can be placed (Fig. 5C). Variation is less than 2% when only the central 4 mm diameter area is employed in this geometry.

The newly designed β -source delivers approximately $0.0375 \text{ Gy s}^{-1} \text{ GBq}^{-1}$ at a distance of 7.45 mm from the source to the top of the 0.5 mm thick target disc in the lexyg system.

The absorbed doses were similar for discs made from brass, nickel and two different varieties of stainless steel, but approximately 15% lower for aluminium. Only for the latter material the dose profile exhibits a different pattern with a pronounced continuous increase in dose starting at ~ 0.8 mm distance from the rim, whereas the other materials show similar patterns as in Fig. 3A, where a maximum is reached towards the edge with a subsequent decrease in dose.

Discussion and conclusions

The uniformity of β -irradiation at sample position is shown to vary between 2 and 8% for areas of 8 and 10 mm diameter centred around flat sample discs, respectively. The variation obtained is significantly lower than some recently reported values (e.g. factor 1.4 in Ballarini et al., 2006), and is considered satisfactory for luminescence dating applications.

For the present source design the reported uniformity could only be achieved by pre-selection of individual miniaturized sources and ensuring a variation in activities of less than 5%. Because of the special source design, in RF application the luminescence signal can be efficiently collected through adapted lens optics without any need for a light guide. The gain in signal intensity is contrasted by an increased dark count due to the proximity of the β -source to the light detector (i.e. PMT or EMCCD).

The 'free in air' experiment, where little influencing material is close to the source, shows the significance of the actual geometry of the irradiation, which includes not only the housing and surrounding materials, but the shape of the substrate as well.

While the radiation field from the source itself was shown to be very homogeneous, inhomogeneities are mainly caused by backscatter effects. Obviously, the material of the sample carrier matters, but the size and shape of sample carrier as well as of the heating plate are influential parameters in the dose distribution. The presence/absence of a rim of the sample carrier has been shown to have a large influence on the homogeneity of the radiation field. Employing a sample carrier with a 0.5 mm rim has a pronounced effect on the homogeneity of the irradiation, leaving only the central 4-6 mm diameter area (of the original 8 mm) available, if homogeneous irradiation is required. Not investigated here are effects arising from the material which is irradiated, as well as from its shape and size.

In any case, it is advisable for irradiation with any non-photon source not to employ the entire surface of a disc/cup in order to avoid inhomogeneities which appear to increase usually towards the edge of the irradiation area (e.g. Spooner and Allsop, 2000). Given the observed influence of the rim when cups are used (Fig. 5), it appears to be prudent to minimize the rim of the cup in order to minimize its effect on the variation of absorbed dose.

The influence of inhomogeneous artificial irradiation on luminescence dating results would merit further investigation and especially with the further developments in small scale luminescence measurements, like single grain and spatially resolved luminescence, such influences are becoming more important. Some of the overdispersion observed in luminescence dating might be attributable to such non-uniformity of β -irradiation. Because of the sufficiently small variation in dose delivered by the current ring source, the lexyg system does not need to be calibrated for single positions (e.g. single grain measurements) and allows a single grain approach, areas of interest of single grains from multiple grain aliquots or for solid samples by e.g. EMCCD luminescence analysis. Due to the uniformity of the

radiation field any random displacements of the sample carrier or sample grains during sample handling in the measuring system are less crucial with respect to absorbed dose, provided the grains are spherical.

Experiments have shown that the commonly observed bell shape of the dose distribution over irradiated area (e.g. Spooner and Allsop, 2000) is mainly due to geometric effects of the irradiation, where the centre is being irradiated by the entire active areas and a uniform irradiation appears to be obtainable when the activity is less in the centre of the source, as is the case with the ring source in the LEXSYG system. The main advantage of the present source design is the homogeneous radiation field as well as the ability for efficient fluorescence light collection through lens optics for RF application.

Acknowledgements

We would like to thank David Sanderson for his constructive comments which improved the paper a lot. This work has been supported by the German Federal Ministry of Economics and Technology (BMW).

References

- Aitken, M.J. (1985). *Thermoluminescence Dating*. Academic Press, London.
- Bailiff, I.K. (1980). A beta irradiator for use in TL dating. *Ancient TL* 10, 12-14.
- Ballarini, M., Wintle, A.G., Wallinga, J. (2006). Spatial variation of dose rate from beta sources as measured using single grains. *Ancient TL* 24, 1-8.
- Bøtter-Jensen, L., Andersen, C.E., Duller, G.A.T., Murray, A.S. (2003). Developments in radiation, stimulation and observation facilities in luminescence measurements. *Radiation Measurements* 37, 535-541.
- Erfurt, G., Krbetschek, M.R., Bortolot, V.J., Preusser, F., (2003). A fully automated multi-spectral radioluminescence reading system for geochronometry and dosimetry. *Nuclear Instruments and Methods in Physics Research B* 207, 487-499.
- Ingram, S., Stokes, S., Bailey, R. (2002). Confirmation of backscattered beta dose enhancement rates based on single aliquot regeneration (SAR) analysis of quartz sand and silt. *Ancient TL* 19, 51-54.
- Lapp, T., Jain, M., Thomsen, K.J., Murray, A.S., Buylaert, J.-P. (2012). New luminescence measurement facilities in retrospective dosimetry. *Radiation Measurements* 47, 803-808.
- Liritzis, Y., Galloway, R. (1990). Bremsstrahlung from a shielded beta irradiator. *Journal of Radioanalytical and Nuclear Chemistry* 146, 333-345.
- Sanderson, D.C.W., Chambers, D.A. (1985). An automated beta irradiator using a Sr-90 foil source. *Ancient TL* 3, 26-29.
- Spooner, N.A., Allsop, A. (2000). The spatial variation of dose-rate from $^{90}\text{Sr}/^{90}\text{Y}$ beta sources for use in luminescence dating. *Radiation Measurements* 32, 49-55.
- Valladas, H., Valladas, G. (1982). Effect de l'irradiation alpha sur des grain de quartz. PACT, *Revue du groupe européen d'études pour les techniques physiques, chimiques et mathématiques appliquées à l'archéologie* 6, 171-179.
- Veronese, I., Shved, V., Shishkina, E.A., Giussani, A., Göksu, H.Y. (2007). Study of dose rate profile at sample disks in a Risø OSL single-grain attachment system. *Radiation Measurements* 42, 138-143.

Reviewer

D.C.W. Sanderson

Reviewers Comment

Uniformity of radiation fields used in calibrating luminescence systems remains of critical importance to analysis and reduction of overall dating errors. Here the idea of using an annular source design instead of a disc based source is discussed. The dose mapping results here are highly encouraging and confirm that this approach partly compensates for the centre-weighted dose distributions achieved with disc sources. The new geometry also offers added potential for observing RL through a central aperture in the source. It will be interesting to see how such systems perform in comparison with existing geometries over a range of dating samples.

Thesis Abstracts

Author: Xiang-Jun Liu
Thesis Title: The Late Quaternary lake level history of Qinghai Lake in NE Tibetan Plateau based on optically stimulated luminescence dating
Grade: Ph.D.
Date: July 2011
Supervisors: Zhong-Ping Lai
Address: Luminescence Dating Group, Qinghai Institute of Salt Lakes, Chinese Academy of Sciences, XiNing, P.R. China

Qinghai Lake is located near the junction of three climate systems (the East Asian monsoon, the Indian monsoon, and the Westerlies) and its location makes it one of the most sensitive regions to climate change in the world. During the past 3 years, we identified paleoshoreline deposits, lacustrine deposits and near shore sands around the lake, and these deposits were covered by later alluvial gravels and loess. Finally, 73 optically stimulated luminescence (OSL) samples were collected from paleoshoreline deposits, lacustrine deposits and near shore sands, 11 OSL samples were collected from fluvial deposits, 6 OSL samples were collected from sand wedges, 23 OSL samples were collected from aeolian sands, and 28 OSL samples were collected from loesses and paleosols. In total, 144 OSL samples were collected.

In this thesis, we report the OSL ages of paleoshoreline deposits, lacustrine deposits, fluvial deposits, alluvial deposits, sand wedges and aeolian deposits around Qinghai Lake. The elevation of paleoshoreline deposits were measured by differential global positioning system (GPS). A lake level fluctuation curve was then constructed from the above measurements. It is concluded that:

- (1) Shoreline deposits and lacustrine sediments all accumulated below 3260 m above sea level (asl) (~66 m above modern lake level).
- (2) The highest lake level for the past 140 ka occurred during MIS 5a (3260 m asl, ~66 m above modern lake level), the lake level in early MIS 3a is 3209 m, ~5 meter higher than the highest Holocene lake level. The highest lake level of Holocene occurred between 8 and 6 ka (3204 m asl, ~9.4 m above modern lake level). Lake levels during MIS 2 and MIS 4 were lower than present, with the lowest lake level occurring during the Last Glaciation Maximum (LGM).

(3) Using GIS software and a digital elevation model (DEM), lake areas in MIS 5a, early MIS 3a, LGM, and Holocene highest period were calculated, the areas were 6753 km², 5238 km², 1225 km² and 4938 km², respectively.

(4) The oldest aeolian deposits around Qinghai Lake are in excess of 165 ka. Surface mantled aeolian deposition then began at ~14 ka. Periods of palaeosol formation occurred at ~16.9 ka, ~12.2-11 ka, ~10-9 ka, ~5.2-4 ka, and ~3.9-0.7 ka. The accumulation intervals of palaeosols are generally consistent with drilling-core-based environmental change proxies, indicating that palaeosols were formed during wet periods with higher vegetation cover.

(5) Sand/ice wedges in Qinghai Lake area formed between 15 and 30 ka, at ~45.5 ka and ~62.4 ka, corresponding to the cold stages. We deduced that the mean annual air temperature (MAAT) would have been depressed by at least 3°C during the past sand/ice wedge formation periods in Qinghai Lake area.

Author: Davinia Moreno
Thesis Title: Datation par ESR de quartz optiquement blanchis (ESR-OB) de la région d'Atapuerca (Burgos, Espagne). Application au site préhistorique de Gran Dolina (contexte karstique) et aux systèmes fluviaux quaternaires de l'Arlanzón et l'Arlanza
Grade: Ph.D.
Date: October 2011
Supervisors: Christophe Falguères, Alfredo Pérez-González and Robert Sala i Ramos
Address: Muséum National d'Histoire Naturelle / UMR 7194 du CNRS Paris, France; Universitat Rovira i Virgili (URV) Tarragona, Spain; Institut Català de Paleoecologia Humana i Evolució Social (IPHES) Tarragona, Spain.

The Sierra de Atapuerca, located in the north-east of the Duero Basin (Northern Spain), is a Mesozoic eroded hill characterized by a well-developed karst system. After the construction of a railway trench

“Trinchera Atapuerca” by a British mining company at the end of the XIX century, an almost continuous hominid occupation has been documented since ~1.2 Ma, through the discovery of a series of major archaeological cave sites, such as Sima del Elefante, Gran Dolina, Sima de los Huesos or Galería, among others. Previous investigations combining geomorphological evolution analysis of the Sierra de Atapuerca landscape and the study of the karst system revealed a connection between the karst formation and the regional fluvial network, particularly on the nearby Arlanzón, Arlanza and Pico rivers.

The chronological framework of the archaeological sites is currently limited to biochronological, palaeomagnetic data and a few absolute dates, while geochronological data are still missing on the fluvial systems. In order to refine the chronological framework of this region and to improve the knowledge of the connexions between the karst system and the fluvial network, we applied the Electron Spin Resonance dating method to optically bleached quartz (ESR-OB) extracted from sediments. These samples were collected from the karstic deposits of the 18m-thick sedimentary sequence of Gran Dolina site and from the terraces systems of the Arlanzón, Arlanza and Pico rivers. While this method has already been successfully used in fluvial context, its application to sediment extracted from karstic infill was still a challenge.

From a methodological point of view, the ESR dating results derived from the analyses of almost 40 samples from Gran Dolina site are consistent with the previous chronostratigraphical framework and thus demonstrate the potential of the ESR-OB for karstic contexts. In addition, these new results provide for the first time absolute dates for the lowermost layers of the Gran Dolina stratigraphic sequence, and suggest that sedimentation in Gran Dolina cave started ~1.2 Ma years ago and it was almost continuous until its complete infilling ~200 ka years ago. It confirms that Gran Dolina site is one of the most important archaeological sites in understanding the earliest occupation of Western Europe. Lastly, the ESR-OB results obtained for the terraces systems are consistent and reinforce the previous chronostratigraphic framework established by the combination of geomorphologic and palaeomagnetic data. These dating results confirm the contemporaneity of the terraces T4_{AZN} and T5_{AZN} in the Arlanzón valley and the human-bearing deposits of Gran Dolina site and help to refine the correlation between the Arlanza and the Arlanzón river systems.

Author: Richard Lyons
Thesis Title: Chronology and controls of Late Quaternary sedimentation, pedogenesis and erosion across interior South Africa
Grade: Ph.D.
Date: February 2012
Supervisors: Stephen Tooth and Geoff Duller
Address: Institute of Geography and Earth Sciences, Aberystwyth University, Aberystwyth, UK

Soil erosion is one of South Africa’s most pressing environmental problems. Across the interior, many river channels are presently incising and dongas (gullies and badland-type terrain) have formed extensively in colluvial and alluvial deposits. However, the chief driver(s) of this present incisional phase is contested. Donga formation has traditionally been attributed to human disturbance (e.g. livestock overgrazing), but evidence for the role of humans is largely circumstantial due to limited knowledge of when present incision initiated. Further, there is a paucity of Late Quaternary chronologies of sedimentation, pedogenesis and erosion with which to contextualise present channel and donga incision.

To establish chronologies of sedimentation, pedogenesis and erosion across interior South Africa, and to constrain when present incision initiated, optically stimulated luminescence (OSL) ages have been determined for colluvial and alluvial sediments associated with dongas at three sites: i) Erfkroon, middle Modder River, Free State; ii) Steelpoort region, Limpopo Province; and iii) upper Blood River region, KwaZulu-Natal. These widely spaced sites are associated with contrasting climates, lithologies, soil types, physiographies and land use histories. Inter-site comparison of the OSL chronologies, and correlation with Late Quaternary environmental and land use changes, provides a novel opportunity to examine the relative importance of local (e.g. local base level fall, soil type) and regional (e.g. climate change) drivers of incision.

The OSL chronologies indicate that alluvial and colluvial sedimentation, with intervening episodes of pedogenesis, have been dominant for at least the last 44 ka, 117 ka and 100 ka at the Modder River, Steelpoort and Blood River sites, respectively. In contrast, channel and donga incision initiated at all three sites within the last 2.7 ka, and no later than 0.22 ka. The present phase of incision appears to be of a greater magnitude than any previous phases of incision in the Late Quaternary sedimentary records at the three sites.

Contrary to the traditional view that incision is driven by human disturbance, the broadly regionally synchronous onset of incision at all three sites predates the main phase of landscape disturbance associated with European population expansion and agricultural intensification during the second half of the 18th century. Instead, incision coincides with abrupt climate changes associated with the Medieval Warm Period (MWP) and the Little Ice Age (LIA). In particular, reduced temperatures, precipitation and vegetation cover during the LIA, combined with the likely occurrence of high-magnitude storms and floods, appears to have resulted in the destabilisation of landsurfaces and the shift from long-term net sedimentation to net erosion. The abruptness of climatic change associated with the LIA appears to have been a crucial factor in initiating incision. Additional controls on the patterns, magnitude and timing of channel and donga incision include soil type and local base level falls that are related to the breaching of resistant rock barriers in channel beds.

Author: Reza Sohbat
Thesis Title: Optically stimulated luminescence dating of rock surfaces
Grade: Ph.D.
Date: May 2012
Supervisor: Andrew Murray
Address: Nordic Laboratory for Luminescence Dating, DTU Risø Campus, Roskilde, 4000 Denmark

There are many examples of rock surfaces, rock art and stone structures whose ages are of great importance to the understanding of various phenomena in geology, climatology and archaeology. Optically stimulated luminescence (OSL) dating is a well-established chronological tool that has successfully determined the depositional age of a wide variety of fine-grained sediments, from several years to several hundred thousands of years. However, there is no routine OSL dating method applicable to larger clasts such as cobbles, boulders and other rock surfaces.

The thesis is a compilation of six articles, an introduction, and a summary chapter. The application of quartz OSL to the dating of rock surfaces is successfully tested by application to two different quartz-rich rock types (sandstone and quartzite). Together with the measurement of infrared stimulated luminescence (IRSL) signals as a function of depth into the surface of different granites it is clear that both OSL and IRSL can be fully reset in the two mm

closest to the rock surface. However, it appears that the sensitivity of quartz from the granitic rocks (the most common surficial rock type) cannot be relied on. Na-rich feldspar is suggested as an alternative dosimeter, using a yellow-emission elevated-temperature IRSL signal.

Based on the studies of residual luminescence as a function of depth into a rock surface discussed above, a model is developed that relates this increase in residual luminescence to the exposure time. The model is then further developed using the quartz OSL signal from buried quartzite cobbles to include the effects of the environmental dose rate. By fitting the model to the dose-depth variation from a single clast, four events (two light exposures of different durations each followed by a burial period) in the history of a single cobble are identified and quantified. However, the use of model parameter estimates based on first principles does not result in the expected exposure times. In an alternative approach a known-age quartz-rich sandstone is used for calibration, and the model is then used to constrain the likely age of an important Native American rock-art style.

It is concluded that the OSL dating of large clasts and rock surfaces in routine applications is practical, and in some ways may be preferable to the dating of finer-grained sediments. Both burial ages and exposure ages can be quantified using this approach, and in a final illustration of this, the model is made suitable for space application by including simultaneous light exposure and irradiation. This offers, for the first time, a practical approach to the establishment of a recent exposure chronology for non-terrestrial surfaces, such as on Mars.

Author: Christina M. Neudorf
Thesis Title: Luminescence investigations into the time of final deposition of Toba volcanic ash and artefact-bearing alluvial sediments in the Middle Son Valley, Madhya Pradesh, India
Grade: PhD
Date: September 2012
Supervisors: Richard G. Roberts, Zenobia Jacobs
Address: Centre for Archaeological Science, University of Wollongong, Gwynneville, NSW, Australia

Terraced alluvial deposits in the Middle Son Valley, Madhya Pradesh, India contain Youngest Toba Tuff (YTT) deposits and an archaeological

record that spans the Acheulean to the Neolithic. For the past three decades, this region has been the focus of geological and archaeological investigations that aim to understand the impact of the ~74 thousand year (ka) Toba volcanic super-eruption on the environment and human populations in India. The research presented in this study is focussed on two main themes: 1) developing and applying luminescence dating techniques to alluvial sediments in the Middle Son Valley to assess the reliability of the YTT ash as a reliable chronostratigraphic marker in palaeoenvironmental investigations; and 2) to test a previously published model of alluvial deposition for the Middle Son Valley near the confluence of the Rehi and Son rivers.

The luminescence dating potential of potassium feldspar (KF) was explored at both the single aliquot and the single grain level for sediments in the Middle Son Valley. KF grains are shown to be suited to single-aliquot regenerative-dose measurement procedures and individual KF grains exhibit fading rates ranging from 0 to more than 20 %/decade. Post-infrared infrared signals (pIRIR) are shown to be less susceptible to anomalous fading, as expected, but evidence presented here suggests that pIRIR ages for alluvial sediments in the Middle Son Valley are less reliable than IRSL ages, because the source traps for these signals are less likely to be completely emptied by sun exposure during transport and deposition in the Son River.

IRSL ages from KF and OSL ages from quartz presented in this study suggest that the final deposition of the sediments above and below the YTT ash deposits in the Middle Son Valley occurred sometime (possibly up to a few tens of thousands of years) after the Toba volcanic super-eruption. This chronology suggests that: 1) the YTT ash has been reworked by fluvial processes and cannot be considered a reliable chronostratigraphic marker as was previously thought; or 2) the YTT ash was deposited soon after the volcanic event ~74 ka ago, but the underlying sediments have since been eroded and replaced by younger, inset fluvial sediments. In both cases, the temporal framework presented here calls into question the validity of previous hypotheses that were based on pedogenic carbonates sampled above, below and within the YTT ash.

A previously published model of alluvial deposition for the Middle Son Valley subdivides its alluvium into five stratigraphic formations. Cross-valley topographic profiles, field observations and IRSL age estimates from terraced alluvial sediments near the Rehi-Son river confluence are used to refine this model. These data not only provide insights into the fluvial history of the Son River and its response to changes in palaeoclimate, but will also inform future archaeological surveys by constraining the

geomorphic context of surficial and excavated artefacts in the area.

This thesis is available as a PDF on the Ancient TL web site www.aber.ac.uk/ancient-tl

Author: Dragan Popov
Thesis Title: The geomorphological evolution of the Tisza River valley in Serbia
Grade: Ph.D.
Date: November 2012
Supervisors: Slobodan B. Marković (OSL research at the Ghent Luminescence Lab under guidance of Dimitri Vandenberghe)
Address: Department of Geography, Faculty of Science, Novi Sad University, Serbia

Tisza is the major tributary of the Danube with respect to length and catchment area. This study focus on the lower section of the Tisza Valley. Sediment successions preserve excellent record of regional climatic, environmental, hydrographic and morphologic changes during the Late Pleistocene and Holocene. From the aspect of fluvial dynamics, the main characteristic is meandering process. The interpretation of evolution in terms of climatic and tectonic forcing has been hampered by the lack of absolute age information in the Serbian part of the valley. Climate changes and neotectonics affected the fluvial activity, which resulted in formation of two units within the Tisza Valley: paleoplain (modified terrace) and floodplain. These units are characterized by intensive fluvial morphology. In this study, the focus is on fluvial dynamics and its chronology. The basis of research was application of optically stimulated luminescence (OSL) dating (first time applied on fluvial sediments in Serbia) and digital elevation model. Older morphology is present on the higher unit, which is verified by OSL dating of terrace sediments. The main aims of OSL were to identify the most promising dosimeter, to document its behaviour and to determine the first reliable chronology of sedimentary processes in the lower Tisza Valley. To achieve these aims 18 samples were collected from a terrace exposure, which consists of a heterogeneous mixture of laminated fluvial sands of the fossilized point bar (the base of terrace) and homogenous loess-like material (the upper part of terrace). For luminescence analysis, the samples were prepared in the usual manner to obtain (180–212 μm)

quartz and K-rich feldspar extracts. The dose rate was determined using gamma spectrometry. The luminescence characteristics of quartz and potassium feldspar were investigated using a SAR protocol. The quartz exhibited a complex behavior. Therefore, detailed investigations were focused on feldspar. After the measurement of test dose signal, a high-temperature IR-stimulation was performed for 100s at 290°C. A dose recovery test was used to test the performance of the SAR-IRSL procedure and to select the most appropriate preheat temperature. Investigations into the behaviour of IRSL measured at 50°C (IR₅₀) showed that preheating in excess of 60s at 225 °C leads to significant sensitivity changes. A preheat of 60s at 115°C was selected from the plateau region and used for D_e determination. The effect of IR stimulation on the thermoluminescence signal and that of preheating on IRSL intensity were examined; the results are inconclusive with respect to thermal stability, but are not inconsistent with the idea that the data do not reflect depletion of an electron trap. The IR₅₀-signal behaves well in the SAR protocol, although it suffers from anomalous fading. There is no clear variation in g-value with depth, and the individual fading rates seem to be spread symmetrically around a mean value of 3.35±0.02% per decade. Observations demonstrate that IRSL dating of feldspar holds potential for establishing a chronology of fluvial dynamics of the Tisa River in Serbia. On two morphological units, meanders are analyzed and their dimensions provide indirect data on bankfull discharges. Based on estimated discharges and elevation, meanders are classified into several generations, which can be explained through the fluvial response to the climate changes. However all generations are not accompanied by separate geomorphologic levels indicating an intensive tectonic subsidence in this part of the Pannonian basin. Based on the theory of fluvial development model, and according to the OSL chronology of sedimentation archive, it can be concluded that Tisza formed meanders of the higher unit (terrace) during the Late Pleistocene. Ages varies little with depth and are consistent with the stratigraphic position of samples (15-15.9 ka) indicating an active fluvial dynamics during the Late Pleistocene. However, four samples collected from the 300-340 cm interval yield distinctly higher ages. The observed inversion led to investigation of D_e distribution in small aliquots. The majority of the results appear to belong to a broad, single population; reflecting the presence of incompletely reset grains. Two samples from the loess-like horizon are the youngest (13-14 ka), which indicates dry environment that followed the end of active fluvial process. It can be concluded that established chronology of sedimentary record supports previous

interpretations of Late Pleistocene origin of this widespread unit of regional geomorphology. Climate warming of the Pleistocene/Holocene transition increased the bankfull discharges, resulting in incision of the floodplain and formation of 8 m riser. Stabilization of the climate in Holocene resulted in formation of small meanders and widening of the low floodplain. However, hydro-regulation interrupted the natural evolution of the Tisza River Valley.

Bibliography

Compiled by Daniel Richter

From 1st June 2012 to 30th November 2012

Ahr, S. W., Nordt, L. C., and Forman, S. L. (2013). Soil genesis, optical dating, and geoarchaeological evaluation of two upland Alfisol pedons within the Tertiary Gulf Coastal Plain. *Geoderma* **192**, 211-226.

Alappat, L., Frechen, M., Tsukamoto, S., and Vink, A. (2012). Reply to ‘Comment on: “Establishing the Late Pleistocene-Holocene sedimentation boundary in the southern North Sea using OSL dating of shallow continental shelf sediments” by L. Alappat, A. Vink, S. Tsukamoto, M. Frechen, Proceedings of the Geologists’ Association 121 (2010), 43-54’ by B. Mauz. *Proceedings of the Geologists’ Association* **123**, 666-668.

Alexanderson, H., and Murray, A. S. (2012). Problems and potential of OSL dating Weichselian and Holocene sediments in Sweden. *Quaternary Science Reviews* **44**, 37-50.

Avnaim-Katav, S., Almogi-Labin, A., Sandler, A., Sivan, D., Porat, N., and Matmon, A. (2012). The chronostratigraphy of a Quaternary sequence at the distal part of the Nile littoral cell, Haifa Bay, Israel. *Journal of Quaternary Science* **27**, 675-686.

Avni, Y., Porat, N., and Avni, G. (2012). Pre-farming environment and OSL chronology in the Negev Highlands, Israel. *Journal of Arid Environments* **86**, 12-27.

Azevedo, R. L., Asfora, V. K., Ribeiro, G. B., Ferreira, J. V. C., Khoury, H. J., Sullasi, H. S. L., Rego, N. J. S., and de Mello, J. A. C. (2012). Archeometric studies in the Franciscan Convent of “Santo Antônio” (Recife, PE). *Applied Radiation and Isotopes* **70**, 2460-2465.

Beckers, B., Schütt, B., Tsukamoto, S., and Frechen, M. (2013). Age determination of Petra's engineered landscape - optically stimulated luminescence (OSL) and radiocarbon ages of runoff terrace systems in the Eastern Highlands of Jordan. *Journal of Archaeological Science* **40**, 333-348.

Berger, G. W., and Polyak, L. (2012). Testing the use of quartz ‘micro-hole’ photon-simulated luminescence for dating sediments from the central Lomonosov Ridge, Arctic Ocean. *Quaternary Geochronology* **11**, 42-51.

Bertrams, M., Protze, J., Löhner, R., Schyle, D., Richter, J., Hilgers, A., Klasen, N., Schmidt, C., and Lehmkuhl, F. (2012). Multiple environmental change at the time of the Modern Human passage through the Middle East: First results from geoarchaeological investigations on Upper Pleistocene sediments in the Wadi Sabra (Jordan). *Quaternary International* **274**, 55-72.

Breman, E., Gillson, L., and Willis, K. (2012). How fire and climate shaped grass-dominated vegetation and forest mosaics in northern South Africa during past millennia. *The Holocene* **22**, 1427-1439.

Briant, R. M., Bates, M. R., Marshall, G. D., Schwenninger, J.-L., and Wenban-Smith, F. F. (2012). Terrace reconstruction and long profile projection: a case study from the Solent river system near Southampton, England. *Proceedings of the Geologists’ Association* **123**, 438-449.

Brill, D., Klasen, N., Jankaew, K., Brueckner, H., Kelleat, D., Scheffers, A., and Scheffers, S. (2012). Local inundation distances and regional tsunami recurrence in the Indian Ocean inferred from luminescence dating of sandy deposits in Thailand. *Natural Hazards and Earth System Sciences* **12**, 2177-2192.

Brown, K. S., Marean, C. W., Jacobs, Z., Schoville, B. J., Oestmo, S., Fisher, E. C., Bernatchez, J., Karkanas, P., and Matthews, T. (2012). An early and enduring advanced technology originating 71,000 years ago in South Africa. *Nature* **491**, 590-593.

- Brown, N. D., and Forman, S. L. (2012). Evaluating a SAR TT-OSL protocol for dating fine-grained quartz within Late Pleistocene loess deposits in the Missouri and Mississippi river valleys, United States. *Quaternary Geochronology* **12**, 87-97.
- Bueno, L., Feathers, J., and De Blasis, P. (2013). The formation process of a paleoindian open-air site in Central Brazil: integrating lithic analysis, radiocarbon and luminescence dating. *Journal of Archaeological Science* **40**, 190-203.
- Bunch, T. E., Hermes, R. E., Moore, A. M. T., Kennett, D. J., Weaver, J. C., Wittke, J. H., DeCarli, P. S., Bischoff, J. L., Hillman, G. C., Howard, G. A., Kimbel, D. R., Kletetschka, G., Lipo, C. P., Sakai, S., Revay, Z., West, A., Firestone, R. B., and Kennett, J. P. (2012). Very high-temperature impact melt products as evidence for cosmic airbursts and impacts 12,900 years ago. *Proceedings of the National Academy of Sciences* **109**, E1903-E1912.
- Burdette, K. E., Rink, W. J., López, G. I., Mallinson, D. J., Parham, P. R., and Reinhardt, E. G. (2012). Geological investigation and optical dating of Quaternary siliciclastic sediments near Apalachicola, North-west Florida, USA. *Sedimentology* **59**, 1836-1849.
- Burgess, W. P., Yin, A., Dubey, C. S., Shen, Z.-K., and Kelty, T. K. (2012). Holocene shortening across the Main Frontal Thrust zone in the eastern Himalaya. *Earth and Planetary Science Letters* **357-358**, 152-167.
- Buylaert, J.-P., Jain, M., Murray, A. S., Thomsen, K. J., Thiel, C., and Sohbaty, R. (2012). A robust feldspar luminescence dating method for Middle and Late Pleistocene sediments. *Boreas* **41**, 435-451.
- Carson, E. C., Hanson, P. R., Attig, J. W., and Young, A. R. (2012). Numeric control on the late-glacial chronology of the southern Laurentide Ice Sheet derived from ice-proximal lacustrine deposits. *Quaternary Research* **78**, 583-589.
- Chapot, M. S., Roberts, H. M., Duller, G. A. T., and Lai, Z. P. (2012). A comparison of natural- and laboratory-generated dose response curves for quartz optically stimulated luminescence signals from Chinese Loess. *Radiation Measurements* **47**, 1045-1052.
- Chapot, M. S., Sohbaty, R., Murray, A. S., Pederson, J. L., and Rittenour, T. M. (2012). Constraining the age of rock art by dating a rockfall event using sediment and rock-surface luminescence dating techniques. *Quaternary Geochronology* **13**, 18-25.
- Clark-Balzan, L. A., Candy, I., Schwenninger, J.-L., Bouzouggar, A., Blockley, S., Nathan, R., and Barton, R. N. E. (2012). Coupled U-series and OSL dating of a Late Pleistocene cave sediment sequence, Morocco, North Africa: Significance for constructing Palaeolithic chronologies. *Quaternary Geochronology* **12**, 53-64.
- Clemmensen, L. B., Nielsen, L., Bendixen, M., and Murray, A. (2012). Morphology and sedimentary architecture of a beach-ridge system (Anholt, the Kattegat sea): a record of punctuated coastal progradation and sea-level change over the past ~1000 years. *Boreas* **41**, 422-434.
- Cohen, T. J., Nanson, G. C., Jansen, J. D., Jones, B. G., Jacobs, Z., Larsen, J. R., May, J. H., Treble, P., Price, D. M., and Smith, A. M. (2012). Late Quaternary mega-lakes fed by the northern and southern river systems of central Australia: Varying moisture sources and increased continental aridity. *Palaeogeography, Palaeoclimatology, Palaeoecology* **356-357**, 89-108.
- Cordier, S., Harmand, D., Lauer, T., Voinchet, P., Bahain, J.-J., and Frechen, M. (2012). Geochronological reconstruction of the Pleistocene evolution of the Sarre valley (France and Germany) using OSL and ESR dating techniques. *Geomorphology* **165-166**, 91-106.
- Cordier, S., Lauer, T., Harmand, D., Frechen, M., and Brkojewitch, G. (2012). Fluvial response to climatic and anthropogenic forcing in the Moselle drainage basin (NE France) during historical periods: Evidence from OSL dating. *Earth Surface Processes and Landforms* **37**, 1167-1175.

- Costa, P. J. M., Leroy, S. A. G., Dinis, J. L., Dawson, A. G., and Kortekaas, S. (2012). Recent high-energy marine events in the sediments of Lagoa de Obidos and Martinhal (Portugal): recognition, age and likely causes. *Natural Hazards and Earth System Sciences* **12**, 1367-1380.
- Cunha, P. P., Almeida, N. A. C., Aubry, T., Martins, A. A., Murray, A. S., Buylaert, J.-P., Sohbati, R., Raposo, L., and Rocha, L. (2012). Records of human occupation from Pleistocene river terrace and aeolian sediments in the Arneiro depression (Lower Tejo River, central eastern Portugal). *Geomorphology* **165-166**, 78-90.
- Cunningham, A. C., DeVries, D. J., and Schaart, D. R. (2012). Experimental and computational simulation of beta-dose heterogeneity in sediment. *Radiation Measurements* **47**, 1060-1067.
- Cunningham, A. C., and Wallinga, J. (2012). Realizing the potential of fluvial archives using robust OSL chronologies. *Quaternary Geochronology* **12**, 98-106.
- Davidovich, U., Porat, N., Gadot, Y., Avni, Y., and Lipschits, O. (2012). Archaeological investigations and OSL dating of terraces at Ramat Rahel, Israel. *Journal of Field Archaeology* **37**, 192-208.
- Delagnes, A., Tribolo, C., Bertran, P., Brenet, M., Crassard, R., Jaubert, J., Khalidi, L., Mercier, N., Nomade, S., Peigné, S., Sitzia, L., Tournepiche, J.-F., Al-Halibi, M., Al-Mosabi, A., and Macchiarelli, R. (2012). Inland human settlement in southern Arabia 55,000 years ago. New evidence from the Wadi Surdud Middle Paleolithic site complex, western Yemen. *Journal of Human Evolution* **63**, 452-474.
- Demeter, F., Shackelford, L. L., Bacon, A.-M., Düringer, P., Westaway, K., Sayavongkhamdy, T., Braga, J., Sichanthongtip, P., Khamdalavong, P., Ponche, J.-L., Wang, H., Lundstrom, C., Patole-Edoumba, E., and Karpoff, A.-M. (2012). Anatomically modern human in Southeast Asia (Laos) by 46 ka. *Proceedings of the National Academy of Sciences* **109**, 14375-14380.
- Diána, N., István, K., Tímea, K., and György, S. (2010). Environmental changes in historical times near Kecel on the Danube-Tisza Interfluvium, Hungary. Archaeological research and Optically Stimulated Luminescence (OSL) dating. *Archeometriai Műhely* **9**, 31-38.
- Dutta, S., Suresh, N., and Kumar, R. (2012). Climatically controlled Late Quaternary terrace staircase development in the fold- and -thrust belt of the Sub Himalaya. *Palaeogeography, Palaeoclimatology, Palaeoecology* **356-357**, 16-26.
- Ekdal, E., Ege, A., Karali, T., and Derin, Z. (2012). Luminescence dating studies of Yeşilova Hoyuk. *Geochronometria* **39**, 268-275.
- Fan, Q., Ma, H., Cao, G., Chen, Z., and Cao, S. (2012). Geomorphic and chronometric evidence for high lake level history in Gahai Lake and Toson Lake of north-eastern Qaidam Basin, north-eastern Qinghai-Tibetan Plateau. *Journal of Quaternary Science* **27**, 819-827.
- Farias, T. M. d. B., and Watanabe, S. (2012). A comparative study of the thermoluminescence properties of several varieties of Brazilian natural quartz. *Journal of Luminescence* **132**, 2684-2692.
- Ferrier, G., and Pope, R. J. J. (2012). Quantitative mapping of alluvial fan evolution using ground-based reflectance spectroscopy. *Geomorphology* **175-176**, 14-24.
- Fitzsimmons, K. E., and Barrows, T. T. (2012). Late Pleistocene aeolian reactivation downwind of the Naracoorte East range, southeastern South Australia. *Zeitschrift Für Geomorphologie* **56**, 225-237.
- Fitzsimmons, K. E., Miller, G. H., Spooner, N. A., and Magee, J. W. (2012). Aridity in the monsoon zone as indicated by desert dune formation in the Gregory Lakes basin, northwestern Australia. *Australian Journal of Earth Sciences* **59**, 469-478.

- Fouache, E., Besenval, R., Cosandey, C., Coussot, C., Ghilardi, M., Huot, S., and Lamothe, M. (2012). Palaeochannels of the Balkh river (northern Afghanistan) and human occupation since the Bronze Age period. *Journal of Archaeological Science* **39**, 3415-3427.
- Fritz, M., Wetterich, S., Schirrmeister, L., Meyer, H., Lantuit, H., Preusser, F., and Pollard, W. H. (2012). Eastern Beringia and beyond: Late Wisconsinan and Holocene landscape dynamics along the Yukon Coastal Plain, Canada. *Palaeogeography, Palaeoclimatology, Palaeoecology* **319-320**, 28-45.
- Gábrís, G., Horváth, E., Novothny, Á., and Ruszkiczay-Rüdiger, Z. (2012). Fluvial and aeolian landscape evolution in Hungary - Results of the last 20 years research. *Geologie en Mijnbouw/Netherlands Journal of Geosciences* **91**, 111-128.
- Galbraith, R. F., and Roberts, R. G. (2012). Statistical aspects of equivalent dose and error calculation and display in OSL dating: An overview and some recommendations. *Quaternary Geochronology* **11**, 1-27.
- Gerlach, R., Fischer, P., Eckmeier, E., and Hilgers, A. (2012). Buried dark soil horizons and archaeological features in the Neolithic settlement region of the Lower Rhine area, NW Germany: Formation, geochemistry and chronostratigraphy. *Quaternary International* **265**, 191-204.
- Giosan, L., Clift, P. D., Macklin, M. G., Fuller, D. Q., Constantinescu, S., Durcan, J. A., Stevens, T., Duller, G.A.T., Tabrez, A. R., Gangal, K., Adhikari, R., Alizai, A., Filip, F., VanLaningham, S., and Syvitski, J. P. M. (2012). Fluvial landscapes of the Harappan civilization. *Proceedings of the National Academy of Sciences* **109**, E1688-E1694.
- Gliganic, L., Jacobs, Z., and Roberts, R. (2012). Luminescence characteristics and dose distributions for quartz and feldspar grains from Mumba rockshelter, Tanzania. *Archaeological and Anthropological Sciences* **4**, 115-135.
- Guérin, G., Discamps, E., Lahaye, C., Mercier, N., Guibert, P., Turq, A., Dibble, H. L., McPherron, S. P., Sandgathe, D., Goldberg, P., Jain, M., Thomsen, K., Patou-Mathis, M., Castel, J.-C., and Soulier, M.-C. (2012). Multi-method (TL and OSL), multi-material (quartz and flint) dating of the Mousterian site of Roc de Marsal (Dordogne, France): correlating Neanderthal occupations with the climatic variability of MIS 5-3. *Journal of Archaeological Science* **39**, 3071-3084.
- Guérin, G., and Mercier, N. (2012). Preliminary insight into dose deposition processes in sedimentary media on a scale of single grains: Monte Carlo modelling of the effect of water on the gamma dose rate. *Radiation Measurements* **47**, 541-547.
- Han, F., Zhang, K., Ji, J., Xu, Y., Chen, F., and Kou, X. (2012). Late Pleistocene sedimentary sequences and paleoclimate changes in Xunhua basin in the upper reach of Yellow River in China. *Frontiers of Earth Science* **6**, 297-305.
- Harding, P., Bridgland, D. R., Allen, P., Bradley, P., Grant, M. J., Peat, D., Schwenninger, J.-L., Scott, R., Westaway, R., and White, T. S. (2012). Chronology of the Lower and Middle Palaeolithic in NW Europe: developer-funded investigations at Dunbridge, Hampshire, southern England. *Proceedings of the Geologists' Association* **123**, 584-607.
- Heggen, H. P., Svendsen, J. I., Mangerud, J., and Lohne, Ø. S. (2012). A new palaeoenvironmental model for the evolution of the Byzovaya Palaeolithic site, northern Russia. *Boreas* **41**, 527-545.
- Hu, Z., Pan, B., Wang, J., Cao, B., and Gao, H. (2012). Fluvial terrace formation in the eastern Fenwei Basin, China, during the past 1.2 Ma as a combined archive of tectonics and climate change. *Journal of Asian Earth Sciences* **60**, 235-245.
- Huang, C. C., Pang, J., Zha, X., Zhou, Y., Su, H., Zhang, Y., Wang, H., and Gu, H. (2012). Holocene palaeoflood events recorded by slackwater deposits along the lower Jinghe River valley, middle Yellow River basin, China. *Journal of Quaternary Science* **27**, 485-493.

- Huckleberry, G., Hayashida, F., and Johnson, J. (2012). New Insights into the Evolution of an Intervalley Prehistoric Irrigation Canal System, North Coastal Peru. *Geoarchaeology* **27**, 492-520.
- Hyatt, O. M., Shulmeister, J., Evans, D. J. A., Thackray, G. D., and Rieser, U. (2012). Sedimentology of a debris-rich, perhumid valley glacier margin in the Rakaia Valley, South Island, New Zealand. *Journal of Quaternary Science* **27**, 699-712.
- Iovita, R., Fitzsimmons, K. E., Dobos, A., Hambach, U., Hilgers, A., and Zander, A. (2012). Dealul Guran: evidence for Lower Palaeolithic (MIS 11) occupation of the Lower Danube loess steppe. *Antiquity* **86**, 973-989.
- Jacobs, Z., Hayes, E. H., Roberts, R. G., Galbraith, R. F., and Henshilwood, C. S. (2013). An improved OSL chronology for the Still Bay layers at Blombos Cave, South Africa: further tests of single-grain dating procedures and a re-evaluation of the timing of the Still Bay industry across southern Africa. *Journal of Archaeological Science* **40**, 579-594.
- Jain, M., Guralnik, B., and Andersen, M. T. (2012). Stimulated luminescence emission from localized recombination in randomly distributed defects. *Journal of Physics: Condensed Matter* **24**, 385402.
- Janssens, M. M., Kasse, C., Bohncke, S. J. P., Greaves, H., Cohen, K. M., Wallinga, J., and Hoek, W. Z. (2012). Climate-driven fluvial development and valley abandonment at the last glacial-interglacial transition (Oude IJssel-Rhine, Germany). *Geologie en Mijnbouw/Netherlands Journal of Geosciences* **91**, 37-62.
- Johnsen, T. F., Olsen, L., and Murray, A. (2012). OSL ages in central Norway support a MIS 2 interstadial (25-20 ka) and a dynamic Scandinavian ice sheet. *Quaternary Science Reviews* **44**, 96-111.
- Kars, R. H., Busschers, F. S., and Wallinga, J. (2012). Validating post IR-IRSL dating on K-feldspars through comparison with quartz OSL ages. *Quaternary Geochronology* **12**, 74-86.
- Kinnaird, T. C., Sanderson, D. C. W., and Woodward, N. L. (2011). Applying luminescence methods to geoarchaeology: a case study from Stronsay, Orkney. *Earth and Environmental Science Transactions of the Royal Society of Edinburgh* **102**, 191-200.
- Kiss, T., Sipos, G., Mauz, B., and Mezősi, G. (2012). Holocene aeolian sand mobilization, vegetation history and human impact on the stabilized sand dune area of the southern Nyírség, Hungary. *Quaternary Research* **78**, 492-501.
- Lancaster, N., and Mahan, S. A. (2012). Holocene dune formation at Ash Meadows National Wildlife Area, Nevada, USA. *Quaternary Research* **78**, 266-274.
- Lauer, T., Krbetschek, M., Mauz, B., and Frechen, M. (2012). Yellow stimulated luminescence from potassium feldspar: Observations on its suitability for dating. *Radiation Measurements* **47**, 974-980.
- Lehmkuhl, F., Hülle, D., and Knippertz, M. (2012). Holocene geomorphic processes and landscape evolution in the lower reaches of the Orkhon River (northern Mongolia). *Catena* **98**, 17-28.
- Li, B., and Li, S.-H. (2012). Determining the cooling age using luminescence-thermochronology. *Tectonophysics* **580**, 242-248.
- Li, Y., Wang, N. a., Li, Z., Zhou, X., and Zhang, C. (2012). Holocene Climate Cycles in Northwest Margin of Asian Monsoon. *Chinese Geographical Science* **22**, 450-461.
- Liritzis, I., and Vafiadou, A. (2012). Calibration aspects of thick source alpha counter ZnS system. *Measurement: Journal of the International Measurement Confederation* **45**, 1966-1980.
- Livingstone, S. J., Evans, D. J. A., Ó Cofaigh, C., Davies, B. J., Merritt, J. W., Huddart, D., Mitchell, W. A., Roberts, D. H., and Yorke, L. (2012). Glaciodynamics of the central sector of the last British-Irish Ice Sheet in Northern England. *Earth-Science Reviews* **111**, 25-55.

- Londoño, A. C., Forman, S. L., Eichler, T., and Pierson, J. (2012). Episodic eolian deposition in the past ca. 50,000 years in the Alto Ilo dune field, southern Peru. *Palaeogeography, Palaeoclimatology, Palaeoecology* **346-347**, 12-24.
- Long, H., Lai, Z., Fuchs, M., Zhang, J., and Li, Y. (2012). Timing of Late Quaternary palaeolake evolution in Tengger Desert of northern China and its possible forcing mechanisms. *Global And Planetary Change* **92-93**, 119-129.
- Lowe, J., Barton, N., Blockley, S., Ramsey, C. B., Cullen, V. L., Davies, W., Gamble, C., Grant, K., Hardiman, M., Housley, R., Lane, C. S., Lee, S., Lewis, M., MacLeod, A., Menzies, M., Müller, W., Pollard, M., Price, C., Roberts, A. P., Rohling, E. J., Satow, C., Smith, V. C., Stringer, C. B., Tomlinson, E. L., White, D., Albert, P., Arienzo, I., Barker, G., Borić, D., Carandente, A., Civetta, L., Ferrier, C., Guadelli, J.-L., Karkanias, P., Koumouzelis, M., Müller, U. C., Orsi, G., Pross, J., Rosi, M., Shalamanov-Korobar, L., Sirakov, N., and Tzedakis, P. C. (2012). Volcanic ash layers illuminate the resilience of Neanderthals and early modern humans to natural hazards. *Proceedings of the National Academy of Sciences* **109**, 13532-13537.
- Lu, H. Y., Wang, X., Wang, X., Sun, X. F., Yi, S. W., Zhou, Y. L., Liu, Q. Y., Swinehart, J., and Vandenberghe, J. (2012). Palaeoclimatic changes in northeastern Qinghai-Tibetan Plateau revealed by magnetostratigraphy and magnetic susceptibility analysis of thick loess deposits. *Geologie en Mijnbouw/Netherlands Journal of Geosciences* **91**, 189-198.
- Mauz, B. (2012). Comment on: "Establishing the Late Pleistocene-Holocene sedimentation boundary in the southern North Sea using OSL dating of shallow continental shelf sediments" by L. Alappat, A. Vink, S. Tsukamoto, M. Frechen, *Proceedings of the Geologists' Association* 121 (2010) 43-54. *Proceedings of the Geologists' Association* **123**, 663-665.
- Mejri, H., Balescu, S., Lamothe, M., Barre, M., Abichou, H., and Bouaziz, S. (2012). Mise en évidence par la luminescence des feldspaths de deux hauts niveaux marins interglaciaires du Pléistocène moyen (MIS 7 et MIS 9) le long de la côte orientale de la Tunisie (Sahel). *Quaternaire* **23**, 175-186.
- Ó Cofaigh, C., Telfer, M. W., Bailey, R. M., and Evans, D. J. A. (2012). Late Pleistocene chronostratigraphy and ice sheet limits, southern Ireland. *Quaternary Science Reviews* **44**, 160-179.
- Oniya, E., Polymeris, G., Tsirliganis, N., and Kitis, G. (2012). Behavior of various Nigerian quartz samples to repeated irradiation and heating. *Geochronometria* **39**, 212-220.
- Ortuño, M., Masana, E., García-Meléndez, E., Martínez-Díaz, J., Štěpančíková, P., Cunha, P. P., Sohbati, R., Canora, C., Buylaert, J.-P., and Murray, A. S. (2012). An exceptionally long paleoseismic record of a slow-moving fault: The Alhama de Murcia fault (Eastern Betic shear zone, Spain). *Geological Society of America Bulletin* **124**, 1474-1494.
- Pánek, T., Šilhán, K., Hradecký, J., Strom, A., Smolková, V., and Zerkal, O. (2012). A megalandslide in the Northern Caucasus foredeep (Uspenskoye, Russia): Geomorphology, possible mechanism and age constraints. *Geomorphology* **177-178**, 144-157.
- Pati, P., Parkash, B., Awasthi, A. K., and Jakhmola, R. P. (2012). Spatial and temporal distribution of inland fans/terminal fans between the Ghaghara and Kosi rivers indicate eastward shift of neotectonic activities along the Himalayan front. A study from parts of the upper and middle Gangetic plains, India. *Earth-Science Reviews* **115**, 201-216.
- Philip, G., Bhakuni, S. S., and Suresh, N. (2012). Late Pleistocene and Holocene large magnitude earthquakes along Himalayan Frontal Thrust in the Central Seismic Gap in NW Himalaya, Kala Amb, India. *Tectonophysics* **580**, 162-177.
- Popov, D., Vandenberghe, D. A. G., and Marković, S. B. (2012). Luminescence dating of fluvial deposits in Vojvodina, N Serbia: First results. *Quaternary Geochronology* **13**, 42-51.

- Ramos, A. M., Cunha, P. P., Cunha, L. S., Gomes, A., Lopes, F. C., Buylaert, J.-P., and Murray, A. S. (2012). The River Mondego terraces at the Figueira da Foz coastal area (western central Portugal): Geomorphological and sedimentological characterization of a terrace staircase affected by differential uplift and glacio-eustasy. *Geomorphology* **165-166**, 107-123.
- Reimann, T., Lindhorst, S., Thomsen, K. J., Murray, A. S., and Frechen, M. (2012). OSL dating of mixed coastal sediment (Sylt, German Bight, North Sea). *Quaternary Geochronology* **11**, 52-67.
- Reimann, T., Thomsen, K. J., Jain, M., Murray, A. S., and Frechen, M. (2012). Single-grain dating of young sediments using the pIRIR signal from feldspar. *Quaternary Geochronology* **11**, 28-41.
- Richter, D., Hublin, J.-J., Jaubert, J., McPherron, S. P., Soressi, M., and Texier, J.-P. (2013). Thermoluminescence dates for the Middle Palaeolithic site of Chez-Pinaud Jonzac (France). *Journal of Archaeological Science* **40**, 1176-1185.
- Richter, D., and Thieme, H. (2012). One first chronometric date for the Lower Palaeolithic occupation at Schöningen 13-I. In "Die chronologische Einordnung der paläolithischen Fundstelle von Schöningen / The chronological setting of the Palaeolithic site of Schöningen." (K.-E. Behre, Ed.), pp. 171-182. Forschungen zur Urgeschichte im Tagebau von Schöningen 1. Verlag des Römisch-Germanischen Zentralmuseums, Mainz.
- Riddiford, N. G., Branch, N. P., Green, C. P., Armitage, S. J., and Olivier, L. (2012). Holocene palaeoenvironmental change and the impact of prehistoric salt production in the Seille Valley, eastern France. *The Holocene* **22**, 831-845.
- Ritz, J. F., Nazari, H., Balescu, S., Lamothe, M., Salamati, R., Ghassemi, A., Shafei, A., Ghorashi, M., and Saidi, A. (2012). Paleoearthquakes of the past 30,000 years along the North Tehran Fault (Iran). *Journal of Geophysical Research* **117**, B06305.
- Robbins, L. H., Campbell, A. C., Brook, G. A., Murphy, M. L., and Hitchcock, R. K. (2012). The Antiquity of the Bow and Arrow in the Kalahari Desert: Bone Points from White Paintings Rock Shelter, Botswana. *Journal of African Archaeology* **10**, 7-20.
- Roberts, D. L., Karkanis, P., Jacobs, Z., Marean, C. W., and Roberts, R. G. (2012). Melting ice sheets 400,000 yr ago raised sea level by 13 m: Past analogue for future trends. *Earth and Planetary Science Letters* **357-358**, 226-237.
- Roeser, P. A., Franz, S. O., Litt, T., Ülgen, U. B., Hilgers, A., Wulf, S., Wennrich, V., Akçer Ön, S., Viehberg, F. A., Çağatay, M. N., and Melles, M. (2012). Lithostratigraphic and geochronological framework for the paleoenvironmental reconstruction of the last ~36 ka cal BP from a sediment record from Lake Iznik (NW Turkey). *Quaternary International* **274**, 73-87.
- Rossetti, D. F., Goes, A. M., Bezerra, F. H. R., Valeriano, M. M., Brito-Neves, B. B., and Ochoa, F. L. (2012). Contribution to the stratigraphy of the onshore Paraíba Basin, Brazil. *Anais da Academia Brasileira de Ciências* **84**, 313-34.
- Roy, N. G., Sinha, R., and Gibling, M. R. (2012). Aggradation, incision and interfluvial flooding in the Ganga Valley over the past 100,000 years: Testing the influence of monsoonal precipitation. *Palaeogeography, Palaeoclimatology, Palaeoecology* **356-357**, 38-53.
- Rozo, M. G., Nogueira, A. C. R., and Truckenbrodt, W. (2012). The anastomosing pattern and the extensively distributed scroll bars in the middle Amazon River. *Earth Surface Processes and Landforms* **37**, 1471-1488.
- Şahiner, E., and Meriç, N. (2012). Infrared stimulated luminescence (IRSL) properties of natural aluminum corrosion. *Geochronometria* **39**, 227-232.
- Saks, T., Kalvans, A., and Zelcs, V. (2012). OSL dating of Middle Weichselian age shallow basin sediments in Western Latvia, Eastern Baltic. *Quaternary Science Reviews* **44**, 60-68.

- Sawakuchi, A. O., Guedes, C. C. F., DeWitt, R., Giannini, P. C. F., Blair, M. W., Nascimento, D. R., and Faleiros, F. M. (2012). Quartz OSL sensitivity as a proxy for storm activity on the southern Brazilian coast during the Late Holocene. *Quaternary Geochronology* **13**, 92-102.
- Scheffers, A., Brill, D., Kelletat, D., Brückner, H., Scheffers, S., and Fox, K. (2012). Holocene sea levels along the Andaman Sea coast of Thailand. *The Holocene* **22**, 1169-1180.
- Schmidt, C., Pettke, T., Preusser, F., Rufer, D., Kasper, H. U., and Hilgers, A. (2012). Quantification and spatial distribution of dose rate relevant elements in silex used for luminescence dating. *Quaternary Geochronology* **12**, 65-73.
- Shen, Z., Törnqvist, T. E., Autin, W. J., Mateo, Z. R. P., Straub, K. M., and Mauz, B. (2012). Rapid and widespread response of the Lower Mississippi River to eustatic forcing during the last glacial-interglacial cycle. *Bulletin of the Geological Society of America* **124**, 690-704.
- Shitaoka, Y., Maemoku, H., and Nagatomo, T. (2012). Quartz OSL dating of sand dunes in Ghaggar Basin, northwestern India. *Geochronometria* **39**, 221-226.
- Shukla, U. K., Srivastava, P., and Singh, I. B. (2012). Migration of the Ganga River and development of cliffs in the Varanasi region, India during the late Quaternary: Role of active tectonics. *Geomorphology* **171-172**, 101-113.
- Simms, A. R., Ivins, E. R., DeWitt, R., Kouremenos, P., and Simkins, L. M. (2012). Timing of the most recent Neoglacial advance and retreat in the South Shetland Islands, Antarctic Peninsula: insights from raised beaches and Holocene uplift rates. *Quaternary Science Reviews* **47**, 41-55.
- Sitzia, L., Bertran, P., Boulogne, S., Brenet, M., Crassard, R., Delagnes, A., Frouin, M., Hatte, C., Jaubert, J., Khalidi, L., Messenger, E., Mercier, N., Meunier, A., Peigne, S., Queffelec, A., Tribolo, C., and Macchiarelli, R. (2012). The Paleoenvironment and Lithic Taphonomy of Shi'Bat Dihya 1, a Middle Paleolithic Site in Wadi Surdud, Yemen. *Geoarchaeology* **27**, 471-491.
- Sohbati, R., Jain, M., and Murray, A. (2012). Surface exposure dating of non-terrestrial bodies using optically stimulated luminescence: A new method. *Icarus* **221**, 160-166.
- Sohbati, R., Murray, A. S., Buylaert, J.-P., Almeida, N. A. C., and Cunha, P. P. (2012). Optically stimulated luminescence (OSL) dating of quartzite cobbles from the Tapada do Montinho archaeological site (east-central Portugal). *Boreas* **41**, 452-462.
- Sohbati, R., Murray, A. S., Chapot, M. S., Jain, M., and Pederson, J. (2012). Optically stimulated luminescence (OSL) as a chronometer for surface exposure dating. *Journal of Geophysical Research - Solid Earth* **117**, B09202.
- St Pierre, E. J., Westaway, K. E., Zhao, J.-x., Gagan, M. K., Lentfer, C., Due, R. A., Morwood, M. J., Hantoro, W. S., Djubiantono, T., and Suwargadi, B. W. (2013). Preliminary U-series and Thermoluminescence dating of excavated deposits in Liang Bua sub-chamber, Flores, Indonesia. *Journal of Archaeological Science* **40**, 148-155.
- Stauch, G., Ijmker, J., Pötsch, S., Zhao, H., Hilgers, A., Diekmann, B., Dietze, E., Hartmann, K., Opitz, S., Wünnemann, B., and Lehmkuhl, F. (2012). Aeolian sediments on the north-eastern Tibetan Plateau. *Quaternary Science Reviews* **57**, 71-84.
- Stolz, C., Huelle, D., Hilgers, A., Grunert, J., Lehmkuhl, F., and Dasch, D. (2012). Reconstructing fluvial, lacustrine and aeolian process dynamics in Western Mongolia. *Zeitschrift Für Geomorphologie* **56**, 267-300.
- Stone, A. E. C., and Bailey, R. M. (2012). The effect of single grain luminescence characteristics on single aliquot equivalent dose estimates. *Quaternary Geochronology* **11**, 68-78.

- Sullivan, M., Field, T. L., Hughes, P., Marwick, B., Przystupa, P., and Feathers, J. K. (2012). OSL ages that inform late phases of dune formation and human occupation near Olympic Dam in northeastern South Australia. *Quaternary Australasia* **29**, 4-11.
- Sun, Y., Lai, Z., Madsen, D., and Hou, G. (2012). Luminescence dating of a hearth from the archaeological site of Jiangxigou in the Qinghai Lake area of the northeastern Qinghai-Tibetan Plateau. *Quaternary Geochronology* **12**, 107-110.
- Tamura, T., Saito, Y., Bateman, M. D., Nguyen, V. L., Ta, T. K. O., and Matsumoto, D. (2012). Luminescence dating of beach ridges for characterizing multi-decadal to centennial deltaic shoreline changes during Late Holocene, Mekong River delta. *Marine Geology* **326-328**, 140-153.
- Tudela, D. R. G., Tatumi, S. H., Yee, M., Brito, S. L. M., Morais, J. L., Morais, D. d., Piedade, S. C., Munita, C. S. P., and Hazenfratz, R. (2012). TL, OSL and C-14 dating results of the sediments and bricks from mummified nuns' grave. *Anais da Academia Brasileira de Ciencias* **84**, 237-44.
- Tunnicliffe, J., Church, M., Clague, J. J., and Feathers, J. K. (2012). Postglacial sediment budget of Chilliwack Valley, British Columbia. *Earth Surface Processes and Landforms* **37**, 1243-1262.
- van Mourik, J. M., Seijmonsbergen, A. C., Slotboom, R. T., and Wallinga, J. (2012). Impact of human land use on soils and landforms in cultural landscapes on aeolian sandy substrates (Maashorst, SE-Netherlands). *Quaternary International* **265**, 74-89.
- Viveen, W., Braucher, R., Bourlès, D., Schoorl, J. M., Veldkamp, A., van Balen, R. T., Wallinga, J., Fernandez-Mosquera, D., Vidal-Romani, J. R., and Sanjurjo-Sanchez, J. (2012). A 0.65 Ma chronology and incision rate assessment of the NW Iberian Miño River terraces based on ¹⁰Be and luminescence dating. *Global And Planetary Change* **94-95**, 82-100.
- Voelkel, J., Murray, A., Leopold, M., and Huerkamp, K. (2012). Colluvial filling of a glacial bypass channel near the Chiemsee (Stottham) and its function as geoarchive. *Zeitschrift Für Geomorphologie* **56**, 371-386.
- Wang, H., Stumpf, A. J., Miao, X., and Lowell, T. V. (2012). Atmospheric changes in North America during the last deglaciation from dune-wetland records in the Midwestern United States. *Quaternary Science Reviews* **58**, 124-134.
- Webb, N. D., Grimley, D. A., Phillips, A. C., and Fouke, B. W. (2012). Origin of glacial ridges (OIS 6) in the Kaskaskia Sublobe, southwestern Illinois, USA. *Quaternary Research* **78**, 341-352.
- Wiwegwin, W., Sugiyama, Y., Hisada, K. I., and Charusiri, P. (2011). Re-evaluation of the activity of the Thoen Fault in the Lampang Basin, northern Thailand, based on geomorphology and geochronology. *Earth, Planets and Space* **63**, 975-990.
- Wygol, B. T., and Goebel, T. (2012). Early Prehistoric Archaeology of the Middle Susitna Valley, Alaska. *Arctic Anthropology* **49**, 45-67.
- Yang, L., Wang, T., Zhou, J., Lai, Z., and Long, H. (2012). OSL chronology and possible forcing mechanisms of dune evolution in the Horqin dunefield in northern China since the Last Glacial Maximum. *Quaternary Research* **78**, 185-196.

Selected papers from the Torun LED'11 conference published in Volume 47/9 of Radiation Measurements

- Arnold, L. J., Demuro, M., and Ruiz, M. N. (2012). Empirical insights into multi-grain averaging effects from 'pseudo' single-grain OSL measurements. *Radiation Measurements* **47**, 652-658.
- Bos, A. J. J., and Wallinga, J. (2012). How to visualize quartz OSL signal components. *Radiation Measurements* **47**, 752-758.

Buylaert, J. P., Jain, M., Murray, A. S., Thomsen, K. J., and Lapp, T. (2012). IR-RF dating of sand-sized K-feldspar extracts: A test of accuracy. *Radiation Measurements* **47**, 759-765.

Clark-Balzan, L., and Schwenninger, J.-L. (2012). First steps toward spatially resolved OSL dating with electron multiplying charge-coupled devices (EMCCDs): System design and image analysis. *Radiation Measurements* **47**, 797-802.

Duller, G. A. T. (2012). Improving the accuracy and precision of equivalent doses determined using the optically stimulated luminescence signal from single grains of quartz. *Radiation Measurements* **47**, 770-777.

Gliganic, L. A., Roberts, R. G., and Jacobs, Z. (2012). Natural variations in the properties of TL and IRSL emissions from metamorphic and volcanic K-feldspars from East Africa: Assessing their reliability for dating. *Radiation Measurements* **47**, 659-664.

Gong, Z., Li, B., and Li, S.-H. (2012). Study of the relationship between infrared stimulated luminescence and blue light stimulated luminescence for potassium-feldspar from sediments. *Radiation Measurements* **47**, 841-845.

Hernandez, M., Mauz, B., Mercier, N., and Shen, Z. (2012). Evaluating the efficiency of TT-OSL SAR protocols. *Radiation Measurements* **47**, 669-673.

Kang, S. G., Wang, X. L., and Lu, Y. C. (2012). The estimation of basic experimental parameters in the fine-grained quartz multiple-aliquot regenerative-dose OSL dating of Chinese loess. *Radiation Measurements* **47**, 674-681.

Lamothe, M., Barré, M., Huot, S., and Ouimet, S. (2012). Natural luminescence and anomalous fading in K-feldspar. *Radiation Measurements* **47**, 682-687.

Lawson, M. J., Roder, B. J., Stang, D. M., and Rhodes, E. J. (2012). OSL and IRSL characteristics of quartz and feldspar from southern California, USA. *Radiation Measurements* **47**, 830-836.

Martini, M., Fasoli, M., Villa, I., and Guibert, P. (2012). Radioluminescence of synthetic and natural quartz. *Radiation Measurements* **47**, 846-850.

Murray, A. S., Thomsen, K. J., Masuda, N., Buylaert, J. P., and Jain, M. (2012). Identifying well-bleached quartz using the different bleaching rates of quartz and feldspar luminescence signals. *Radiation Measurements* **47**, 688-695.

Neudorf, C. M., Roberts, R. G., and Jacobs, Z. (2012). Sources of overdispersion in a K-rich feldspar sample from north-central India: Insights from De, K content and IRSL age distributions for individual grains. *Radiation Measurements* **47**, 696-702.

Nian, X., Bailey, R. M., and Zhou, L. (2012). Investigations of the post-IR IRSL protocol applied to single K-feldspar grains from fluvial sediment samples. *Radiation Measurements* **47**, 703-709.

Pagonis, V., Jain, M., Murray, A. S., Ankjærgaard, C., and Chen, R. (2012). Modeling of the shape of infrared stimulated luminescence signals in feldspars. *Radiation Measurements* **47**, 870-876.

Panzeri, L., Martini, M., and Sibilia, E. (2012). Effects of thermal treatments on luminescence features of three natural feldspars. *Radiation Measurements* **47**, 877-882.

Qin, J. T., and Zhou, L. P. (2012). Effects of thermally transferred signals in the post-IR IRSL SAR protocol. *Radiation Measurements* **47**, 710-715.

Roberts, H. M. (2012). Testing Post-IR IRSL protocols for minimising fading in feldspars, using Alaskan loess with independent chronological control. *Radiation Measurements* **47**, 716-724.

Thomsen, K. J., Murray, A., and Jain, M. (2012). The dose dependency of the over-dispersion of quartz OSL single grain dose distributions. *Radiation Measurements* **47**, 732-739.

Timar-Gabor, A., Vasiliniuc, Ș., Vandenberghe, D. A. G., Cosma, C., and Wintle, A. G. (2012). Investigations into the reliability of SAR-OSL equivalent doses obtained for quartz samples displaying dose response curves with more than one component. *Radiation Measurements* **47**, 740-745.

Tsukamoto, S., Jain, M., Murray, A., Thiel, C., Schmidt, E., Wacha, L., Dohrmann, R., and Frechen, M. (2012). A comparative study of the luminescence characteristics of polymineral fine grains and coarse-grained K- and Na-rich feldspars. *Radiation Measurements* **47**, 903-908.

Westaway, K., and Prescott, J. (2012). Investigating signal evolution: A comparison of red and UV/blue TL, and UV OSL emissions from the same quartz sample. *Radiation Measurements* **47**, 909-915.

Selected papers from the Torun LED'11 conference published in Volume 10 of Quaternary Geochronology

Alexanderson, H., and Murray, A. S. (2012). Luminescence signals from modern sediments in a glaciated bay, NW Svalbard. *Quaternary Geochronology* **10**, 250-256.

Barré, M., Lamothe, M., Backwell, L., and McCarthy, T. (2012). Optical dating of quartz and feldspars: A comparative study from Wonderkrater, a Middle Stone Age site of South Africa. *Quaternary Geochronology* **10**, 374-379.

Bateman, M. D., Swift, D. A., Piotrowski, J. A., and Sanderson, D. C. W. (2012). Investigating the effects of glacial shearing of sediment on luminescence. *Quaternary Geochronology* **10**, 230-236.

Brodard, A., Guibert, P., Lévêque, F., Mathé, V., Carozza, L., and Burens, A. (2012). Thermal characterization of ancient hearths from the cave of Les Fraux (Dordogne, France) by thermoluminescence and magnetic susceptibility measurements. *Quaternary Geochronology* **10**, 353-358.

Cao, G., Long, H., Zhang, J., and Lai, Z. (2012). Quartz OSL dating of last glacial sand dunes near Lanzhou on the western Chinese Loess Plateau: A comparison between different granulometric fractions. *Quaternary Geochronology* **10**, 32-36.

Constantin, D., Timar-Gabor, A., Veres, D., Begy, R., and Cosma, C. (2012). SAR-OSL dating of different grain-sized quartz from a sedimentary section in southern Romania interbedding the Campanian Ignimbrite/Y5 ash layer. *Quaternary Geochronology* **10**, 81-86.

Fan, A., Li, S.-H., and Chen, Y.-G. (2012). Late pleistocene evolution of Lake Manas in western China with constraints of OSL ages of lacustrine sediments. *Quaternary Geochronology* **10**, 143-149.

Fu, X., Li, B., and Li, S.-H. (2012). Testing a multi-step post-IR IRSL dating method using polymineral fine grains from Chinese loess. *Quaternary Geochronology* **10**, 8-15.

Fuchs, M., Kreutzer, S., Fischer, M., Sauer, D., and Sørensen, R. (2012). OSL and IRSL dating of raised beach sand deposits along the southeastern coast of Norway. *Quaternary Geochronology* **10**, 195-200.

Hasebe, N., Inagaki, A., Endo, N., Fukushi, K., Ito, K., and Kashiwaya, K. (2012). Thermoluminescence color image analysis of sediments from Lake Khuvsgul, Mongolia, and its potential to investigate paleoenvironmental change. *Quaternary Geochronology* **10**, 156-159.

Hou, G., Lai, Z., Sun, Y., and Ye, M. (2012). Luminescence and radiocarbon chronologies for the Xindian Culture site of Lamafeng in the Guanting Basin on the NE edge of the Tibetan Plateau. *Quaternary Geochronology* **10**, 394-398.

Huot, S., and Lamothe, M. (2012). The implication of sodium-rich plagioclase minerals contaminating K-rich feldspars aliquots in luminescence dating. *Quaternary Geochronology* **10**, 334-339.

- Jeong, G. Y., and Choi, J.-H. (2012). Variations in quartz OSL components with lithology, weathering and transportation. *Quaternary Geochronology* **10**, 320-326.
- Kadereit, A., DeWitt, R., and Johnson, T. C. (2012). Luminescence properties and optically (post-IR blue-light) stimulated luminescence dating of limnic sediments from northern Lake Malawi - Chances and limitations. *Quaternary Geochronology* **10**, 160-166.
- Kreutzer, S., Fuchs, M., Meszner, S., and Faust, D. (2012). OSL chronostratigraphy of a loess-palaeosol sequence in Saxony/Germany using quartz of different grain sizes. *Quaternary Geochronology* **10**, 102-109.
- Li, B., and Li, S.-H. (2012). Luminescence dating of Chinese loess beyond 130 ka using the non-fading signal from K-feldspar. *Quaternary Geochronology* **10**, 24-31.
- Liu, J., Murray, A. S., Jain, M., Buylaert, J.-P., Lu, Y., and Chen, J. (2012). Developing a SAR TT-OSL protocol for volcanically-heated aeolian quartz from Datong (China). *Quaternary Geochronology* **10**, 308-313.
- Molodkov, A. (2012). Cross-check of the dating results obtained by ESR and IR-OSL methods: Implication for the Pleistocene palaeoenvironmental reconstructions. *Quaternary Geochronology* **10**, 188-194.
- Reimann, T., and Tsukamoto, S. (2012). Dating the recent past (500 years) by post-IR IRSL feldspar - Examples from the North Sea and Baltic Sea coast. *Quaternary Geochronology* **10**, 180-187.
- Rittenour, T. M., Riggs, N. R., and Kennedy, L. E. (2012). Application of single-grain OSL to date quartz xenocrysts within a basalt flow, San Francisco volcanic field, northern Arizona, USA. *Quaternary Geochronology* **10**, 300-307.
- Russell, N. J., and Armitage, S. J. (2012). A comparison of single-grain and small aliquot dating of fine sand from Cyrenaica, northern Libya. *Quaternary Geochronology* **10**, 62-67.
- Schatz, A.-K., Buylaert, J.-P., Murray, A., Stevens, T., and Scholten, T. (2012). Establishing a luminescence chronology for a palaeosol-loess profile at Tokaj (Hungary): A comparison of quartz OSL and polymineral IRSL signals. *Quaternary Geochronology* **10**, 68-74.
- Stang, D. M., Rhodes, E. J., and Heimsath, A. M. (2012). Assessing soil mixing processes and rates using a portable OSL-IRSL reader: Preliminary determinations. *Quaternary Geochronology* **10**, 314-319.
- Thiel, C., Buylaert, J.-P., Murray, A. S., Elmejdoub, N., and Jedoui, Y. (2012). A comparison of TT-OSL and post-IR IRSL dating of coastal deposits on Cap Bon peninsula, north-eastern Tunisia. *Quaternary Geochronology* **10**, 209-217.
- Trauerstein, M., Lowick, S., Preusser, F., Rufer, D., and Schlunegger, F. (2012). Exploring fading in single grain feldspar IRSL measurements. *Quaternary Geochronology* **10**, 327-333.
- Vasiliniuc, Ș., Vandenbergh, D. A. G., Timar-Gabor, A., Panaiotu, C., Cosma, C., and van den Haute, P. (2012). Testing the potential of elevated temperature post-IR IRSL signals for dating Romanian loess. *Quaternary Geochronology* **10**, 75-80.
- Wu, T.-S., Kunz, A., Jaiswal, M. K., and Chen, Y.-G. (2012). A feasibility study on the application of luminescence dating for quartz from different rock types as a thermochronometer. *Quaternary Geochronology* **10**, 340-344.
- Yang, H., Chen, J., Thompson, J. A., and Liu, J. (2012). Optical dating of the 12 May 2008, Ms 8.0 Wenchuan earthquake-related sediments: Tests of zeroing assumptions. *Quaternary Geochronology* **10**, 273-279.
- Zhao, J., Lai, Z., Liu, S., Song, Y., Li, Z., and Yin, X. (2012). OSL and ESR dating of glacial deposits and its implications for glacial landform evolution in the Bogeda Peak area, Tianshan range, China. *Quaternary Geochronology* **10**, 237-243.

Obituary

Matthias R. Krbetschek (1956-2012)

On October 14th, 2012 we lost not only a dear friend but also a distinguished colleague in the field of luminescence dating and geochronology.

After a prolonged period of illness, Matthias Krbetschek finally passed away at his home in Freiberg (Germany) on October 14th, 2012. He will not only be remembered for his outstanding professional achievements in the development and application of luminescence dating techniques, documented by almost 80 scientific publications, but especially for his kindness and personality. Matthias was always willing to help, share his knowledge and also happy to share a beer or two. While he certainly was not a person of many words, he always considered his words carefully.

Matthias R. Krbetschek was born in Frankenberg (Saxony, GDR) in 1956. After school he was trained as a mechanic, while receiving his university entry diploma, which was a specific form of education in former East Germany. Then he joined the *University of Freiberg* and received a degree in geology on tin deposits in 1982. Subsequently he worked for almost 5 years as a geological research assistant in the Lausitz lignite field, doing research on the Quaternary sediments for the exploration research department of the state run open air lignite mining company. During this time he developed his interest in obtaining age estimates for these sediments and therefore went back to the *Technical University of Freiberg* to pursue a doctoral thesis.

These interests led to the set up of the first luminescence dating laboratory of the former "German Democratic Republic" in 1988, located at the department for *Applied Physics* at the *Technical University of Freiberg*. This was made possible within the framework of the project "*Contributions through natural radioactivity and geochronology to environmental and climatic studies*" of the *Saxonian Academy of Science* (SAW). For training and scientific exchange Matthias went to Estonia in 1989 to work with the late Galina Hütt and performed the first luminescence dating for East German sediments. Immediately after German reunification, in 1990, Matthias sought contact with West German and international scientists working in luminescence dating. A strong relationship between his laboratory and the Luminescence laboratory of the *Heidelberg Academy of Science* at the *Max-Planck Institute for*



Nuclear Physics in Heidelberg (Germany) developed, which culminated in a large project on luminescence spectroscopy within the framework of the scheme '*New technologies for the humanities*', funded by the German *Ministry of Education and Research* (BMBF). As a result of these close contacts a regular meeting of the Heidelberg and Freiberg luminescence groups was established, which later became the '*German Luminescence and ESR dating Meeting*'. Many friendships with Matthias developed during the hiking in any wind and weather, which traditionally takes place at these meetings.

In 1993 the project in Freiberg was diversified, receiving a long term funding by the '*Sächsische Akademie der Wissenschaften*' (SAW), and the operational part of the branch '*Quaternary Geochronology*' was led by Matthias. He was awarded the title *doctor rerum naturarum* (Dr. rer. nat.) by the faculty of *Geosciences, Geotechnics and Mining* of the *Technical University of Freiberg* in 1995 for his thesis entitled '*Luminescence dating of quaternary sediments from Central, East and Northern Germany*'.

Matthias' interests were widely spread and his fundamental background in physics was essential not only for his work, but also for the many colleagues who sought his advice and he was always willing to share his knowledge. Much of his efforts were dedicated to fundamental research on luminescence emissions, but he also got involved in assessing the impact of disequilibrium upon dosimetry, together with his dating work in many parts of the world. His

keen interest in Pleistocene ice margins led him to work in Russia and Kamchatka, the Lena delta and various other places, often in collaboration with renowned institutions, such as the Alfred-Wegener Institute. He has provided a major contribution to our knowledge of the age of western European interglacials as well as ice advances during glacial times, often related to archaeological or palaeoanthropological questions.

One of his major achievements was the development of infrared radiofluorescence (IR-RF) dating as the result of a series of PhDs at his laboratory and at the TU Freiberg. Matthias was always open for new technological and technical challenges, like luminescence spectroscopy or detection of luminescence in the yellow wavelength band and also using yellow stimulation. Many of his achievements were obtained through his supervision of many theses from different institutions throughout his career.

Probably the most striking character of his personality was his friendliness and openness to everybody, which, for example, made him decide within a few hours of knowing one of us to travel around Turkey together for almost a week, following the Archaeometry'94 conference in Ankara.

After funding by SAW expired, Matthias started working for the company '*Freiberg Instruments*' in 2011 and gave proof of his innovativeness by designing a new luminescence reader, named 'lexsyg'. During this time he fell ill and was not able to fulfil his duties in continuing his luminescence work in Freiberg within his new position at the *Senckenberg Museum for Mineralogy and Geology* (Dresden) starting in 2012.

Matthias will be remembered as a distinguished colleague by all who knew him, and by many of those as a very dear friend.

Daniel Richter and Ludwig Zöller

Geographisches Institut
Lehrstuhl Geomorphologie
University of Bayreuth

Conference Announcements



University of
St Andrews

600
YEARS

UK Luminescence and ESR meeting

28th-30th August 2013

The 2013 UK Luminescence and ESR dating meeting will be held at the University of St Andrews. Oral and poster presentations covering the physics of luminescence and ESR, methodological issues, and dating applications are all welcome. Research students are particularly encouraged to present.

More details on the conference will be made available in January through the conference website (earthsci.st-andrews.ac.uk/uklum2013.html).

We look forward to seeing you in St Andrews next year.

Ruth Robinson, Adrian Finch, Catherine Brown

E-mail: uklum2013@st-andrews.ac.uk

Book of abstracts for UK Luminescence meeting 2012

UK Luminescence and ESR meeting

The book of abstracts for all the scientific presentations at the UK Luminescence and ESR dating meeting held at Aberystwyth University in September 2012 can be downloaded from the Aberystwyth Luminescence Research Laboratory web site (www.aber.ac.uk/en/iges/research-groups/quatarnary/luminescence-research-laboratory/related-conferences/)

Submission of articles to Ancient TL

Reviewing System

In order to ensure acceptable standards and minimize delay in publication, a modification of the conventional refereeing system has been devised for Ancient TL:

Articles can be sent directly by authors to a member of the Reviewers Panel chosen on the basis of the subject matter, but who is not in any of the authors' laboratories. **At the discretion of the Editor**, reviewers who are not listed in the Panel may be used.

The reviewing system aims to encourage direct dialogue between author and reviewer. The Editor should be kept advised of the progress of articles under review by sending him copies of all correspondence. He is available for advice where reviewing difficulties have arisen. Authors whose mother tongue is not English are required to have their manuscript revised for English *before* submitting it.

We ask reviewers to specify (where required) the minimum of revision that is consistent with achieving a clear explanation of the subject of the paper, the emphasis being on *rapid* publication; reviewers are encouraged to make a brief written comment for publication at the end of the paper. Where a contribution is judged not to meet an adequate standard without substantial modification, the author will be advised that the contribution is not suitable for publication. Articles that are not considered to be of sufficient interest may also be rejected.

Procedures

1. Articles should be submitted to an appropriate member of the Reviewing Panel or Editorial Board, chosen on the basis of the subject matter, but who is not in any of the authors' laboratories.
2. Articles should not normally exceed the equivalent of 5000 words inclusive of diagrams, tables and references. Greater space will be appropriate for certain topics; for these the Editor should first be consulted.
Short notes and letters are also invited. These should not exceed two printed pages in Ancient TL, including diagrams, tables and references (equivalent to ~1400 words of text).
3. Diagrams and labels should be ready for direct reproduction and not normally exceed 12 cm wide by 10 cm high. Where possible, high quality electronic versions of figures should be submitted. Separate figure captions should be supplied. Inappropriately scaled drawings and labels will be returned for alteration.
4. Authors are asked to submit the paper, including diagrams, to the Reviewer and a duplicate copy to the Editor.
The final version of the text must be submitted to the Editor electronically using a standard format (Microsoft Word for PC is currently used for producing Ancient TL). Electronic copies of Diagrams and Tables should also be submitted.
5. Upon receipt of an article, the Editor will send an acknowledgement to the author. If the Reviewer is unable to deal with the contribution within **4 weeks** he/she will inform the author and advise the Editor.

Requirements under various situations

When agreement concerning an article has been reached:

The Editor should receive a copy of the final version of the paper, both as hard copy and electronically. The Reviewer should send their final decision, including comments for publication if any, to the Editor.

If the article has not been rejected, but agreement on its final form cannot be reached or where there are protracted delays in the reviewing process:

The Editor may request an assessment from the Reviewer and responsibility passes to the Editor.

If the article is rejected:

The Editor and author receive notification from the Reviewer, with an indication of the reason for rejection.

Thesis abstracts are to be sent to the Editor and in principle do not need reviewing. However, authors are requested to make sure that the English is correct before submission. Thesis abstracts should not exceed 750 words, and figures and tables are not accepted.

Advertising. Formal information on equipment can be published in Ancient TL. It should not exceed one printed page. Current charges are displayed on the website (<http://www.aber.ac.uk/ancient-tl>)

Subscriptions to Ancient TL

Ancient TL is published 2 times a year and is sent Airmail to subscribers outside the United Kingdom. While every attempt will be made to keep to publication schedule, the Editorial Board may need to alter the number and frequency of issues, depending on the number of available articles which have been accepted by reviewers.

The subscription rate for 2013 is £15 for individual subscribers and £25 for Institutional subscription, plus any taxes where required. Payment must be in pounds sterling. Enquiries and orders must be sent to the Editor. Payment may be by cheques, made payable to 'Aberystwyth University', by credit/debit cards or by bank transfers. Further information on subscriptions is available on the Ancient TL web site (<http://www.aber.ac.uk/ancient-tl>)